Neurobiology of Disease 70 (2014) 53–68

Contents lists available at ScienceDirect

Neurobiology of Disease

journal homepage: www.elsevier.com/locate/ynbdi

Loss of CDKL5 impairs survival and dendritic growth of newborn neurons by altering AKT/GSK-3β signaling

Claudia Fuchs [a], Stefania Trazzi [a], Roberta Torricella [b], Rocchina Viggiano [a], Marianna De Franceschi [a], Elena Amendola [c], Cornelius Gross [c], Laura Calzà [b], Renata Bartesaghi [a], Elisabetta Ciani [a,*]

[a] Department of Biomedical and Neuromotor Sciences, University of Bologna, Italy
[b] Health Sciences and Technologies–Interdepartmental Center for Industrial Research (HST-ICIR), University of Bologna, Italy
[c] Mouse Biology Unit, European Molecular Biology Laboratory (EMBL), Monterotondo, Italy

ARTICLE INFO

Article history:
Received 19 February 2014
Revised 22 May 2014
Accepted 9 June 2014
Available online 18 June 2014

Keywords:
CDKL5 disorder
Rett's syndrome
Neurodevelopmental disorders
Neurogenesis impairment
Dendritic development
AKT/GSK-3β signaling

ABSTRACT

Mutations in the X-linked cyclin-dependent kinase-like 5 (*CDKL5*) gene have been identified in a neurodevelopmental disorder characterized by early-onset intractable seizures, severe developmental delay, intellectual disability, and Rett's syndrome-like features. Since the physiological functions of CDKL5 still need to be elucidated, in the current study we took advantage of a new Cdkl5 knockout (KO) mouse model in order to shed light on the role of this gene in brain development. We mainly focused on the hippocampal dentate gyrus, a region that largely develops postnatally and plays a key role in learning and memory. Looking at the process of neurogenesis, we found a higher proliferation rate of neural precursors in Cdkl5 KO mice in comparison with wild type mice. However, there was an increase in apoptotic cell death of postmitotic granule neuron precursors, with a reduction in total number of granule cells. Looking at dendritic development, we found that in Cdkl5 KO mice the newly-generated granule cells exhibited a severe dendritic hypotrophy. In parallel, these neurodevelopmental defects were associated with impairment of hippocampus-dependent memory. Looking at the mechanisms whereby CDKL5 exerts its functions, we identified a central role of the AKT/GSK-3β signaling pathway. Overall our findings highlight a critical role of CDKL5 in the fundamental processes of brain development, namely neuronal precursor proliferation, survival and maturation. This evidence lays the basis for a better understanding of the neurological phenotype in patients carrying mutations in the *CDKL5* gene.

Introduction

Mutations in the *CDKL5* (cyclin-dependent kinase-like 5) gene are associated with a severe X-linked neurodevelopmental disorder characterized by severe intellectual disability, generalized developmental delay, early-onset intractable seizures, infantile spasms, and Rett's syndrome (RTT)-like features. This condition affects mostly girls and, due to the numerous features that overlap with RTT, it has initially been termed a variant of RTT (Evans et al., 2005; Scala et al., 2005; Tao et al., 2004; Weaving et al., 2004). RTT is a neurodevelopmental disorder that affects young females and shares mental retardation, hyperventilation, hand stereotypies and hypotonia with CDKL5-related disorder. The majority of RTT cases are heterozygous for missense or nonsense mutations in the gene encoding for methyl-CpG-binding protein 2 (MeCP2) (Cheadle et al., 2000). Several *CDKL5* gene mutations, resulting in missense, nonsense, splice, and frameshift mutations or genomic deletions have been described in girls (heterozygous mutations) and a few boys, with all subjects presenting early onset intractable seizures (Bahi-Buisson et al., 2008a, 2008b). Due to the different *CDKL5* mutations and the variable X inactivation in females, the phenotypic spectrum of the disease spans from milder forms—which include the possibility of autonomous walking and less severe epilepsy that is amenable to control—to severe forms featuring intractable seizures, more severe microcephaly and the absence of motor milestones. The male phenotype always falls in the severe spectrum form (Guerrini and Parrini, 2012).

CDKL5, also known as STK9, is a serine/threonine protein kinase that maps to chromosome region Xp22 region. The *CDKL5* gene is composed of 20 coding exons and codes for a protein of 1030 amino acids (Mari et al., 2005). Mutations in the *CDKL5* gene are mainly located within the catalytic domain, strongly suggesting that impaired CDKL5 catalytic activity may play an important role in the pathogenesis of this encephalopathy (Bahi-Buisson et al., 2012; Tao et al., 2004). Thus, knowledge of the molecular targets of CDKL5 may help shed light on the role of CDKL5 in neurodevelopment. The CDKL5 substrates identified so far are DNA methyltransferase 1 (DNMT1) (Kameshita et al., 2008), MeCP2

* Corresponding author at: Department of Biomedical and Neuromotor Sciences, Piazza di Porta San Donato 2, 40126 Bologna, Italy. Fax: +39 051 2091737.
E-mail address: elisabetta.ciani@unibo.it (E. Ciani).
Available online on ScienceDirect (www.sciencedirect.com).

http://dx.doi.org/10.1016/j.nbd.2014.06.006

(Bertani et al., 2006; Mari et al., 2005) and Amphiphysin 1 (Sekiguchi et al., 2013), indicating that CDKL5 may regulate targets both at the nuclear (DNMT1 and MeCP2) and cytoplasmatic level. Moreover, CDKL5 has been shown to bind to the scaffolding protein postsynaptic density (PSD)-95 and to the synaptic cell adhesion molecule NGL-1, thereby influencing dendritic spine formation and growth (Ricciardi et al., 2012; Zhu et al., 2013). This is in agreement with a recent loss-of-function study using RNA interference (RNAi) showing that CDKL5 is required for neurite growth (Chen et al., 2010).

CDKL5 is highly expressed in the brain, mainly in neurons with both a nuclear and dendrite localization (Chen et al., 2010; Ricciardi et al., 2012; Rusconi et al., 2008; Zhu et al., 2013). In the early postnatal period, CDKL5 brain expression exhibits a peak (Ricciardi et al., 2012; Zhu et al., 2013), suggesting its potential importance in brain maturation and function. However, the role/s of CDKL5 in brain development and the molecular mechanisms whereby CDKL5 exerts its effects are still largely unknown. Recently, Cdkl5 knockout (KO) mouse models have been created (Amendola et al., 2014; Wang et al., 2012), in order to understand the etiology of the CDKL5 disorder phenotype. A first characterization of these mice showed that loss of CDKL5 results in autistic-like behavioral abnormalities, decreased dendritic branching of cortical neurons, impairment of neural circuit communication, and alterations in AKT-mTor-S6 pathway (Amendola et al., 2014; Wang et al., 2012).

Using neuroblastoma cell lines as a neuronal model, we recently found that CDKL5 affects both neurite growth and cell proliferation (Valli et al., 2012), suggesting that CDKL5 may modulate not only dendritic maturation, as shown by Chen et al. (2010) but also cell proliferation in the developing brain. In rodents, the hippocampal dentate gyrus produces its neurons mainly postnatally (Aimone et al., 2010; O'Kusky et al., 2000). This makes the hippocampus an ideal structure for the examination of the role of CDKL5 on fundamental neurodevelopmental processes such as neurogenesis and dendritic development. In the current study we used a Cdkl5 KO mouse model in order to dissect the role of CDKL5 in hippocampal development and to establish the mechanism/s underlying its actions. Because of the novelty of this model we have included in our study homozygous and heterozygous females and hemizygous males, in order to clarify the genotype-related severity of the phenotype.

Materials and methods

Colony

Mice for testing were produced by crossing Cdkl5 KO +/− females with Cdkl5 KO Y/− males and Cdkl5 KO +/− females with Y/+ males (Amendola et al., 2014). Littermate controls were used for all experiments. Animals were karyotyped by PCR on genomic DNA using the following primers: 108 F: 5′-ACGATAGAAATAGAGGATCAACCC-3′, 109R: 5′ CCCAAGTATACCCCTT TCCA-3′; 125R: 5′-CTGTGACTAGGGGCTAGA GA-3′. The day of birth was designed as postnatal day (P) zero and animals with 24 h of age were considered as 1-day-old animals (P1). After weaning, mice were housed three to five per cage on a 12-h light/dark cycle in a temperature-controlled environment with food and water provided *ad libitum*. Experiments were performed in accordance with the Italian and European Community law for the use of experimental animals and were approved by Bologna University Bioethical Committee. In this study all efforts were made to minimize animal suffering and to keep the number of animals used to a minimum. A total of 128 animals were used. Supplementary Table 1 summarizes the different experimental groups, their genotype, sex and the experimental procedures used.

BrdU injection

On P40, some animals received one daily intraperitoneal injection (150 μg/g body weight) of BrdU (5-bromo-2-deoxyuridine; Sigma) in 0.9% NaCl solution for five consecutive days. Animals were sacrificed either 24 h after the last BrdU injection (on P45) or after 1 month (on P75) (Supplementary Table 1).

Histological procedures

Some animals (Supplementary Table 1) were deeply anesthetized with ether and transcardially perfused with ice cold phosphate-buffered saline (PBS), followed by a 4% solution of paraformaldehyde in 100 mM PBS, pH 7.4. Brains were stored in the fixative for 24 h, cut along the midline and kept in 20% sucrose in phosphate buffer for an additional 24 h. Hemispheres were frozen and stored at −80 °C. The right hemisphere was cut with a freezing microtome into 30-μm-thick coronal sections that were serially collected in antifreeze solution containing sodium azide. Some animals (Supplementary Table 1) were decapitated and the brain was removed, cut along the midline and fixed by immersion in Glyo-Fixx (Thermo Electron Corp., Waltham, MA, USA) for 48 h. Samples were dehydrated through a series of ascending ethanol concentrations, embedded in paraffin, and cut with a microtome into ultra-thin sections (4 μm) and mounted on poly-lysine slides.

Sections from the dentate gyrus (DG) and subventricular zone (SVZ) were used for immunohistochemistry and Nissl staining. The SVZ of this study corresponds to the rostral horn of the lateral ventricle and starts at the rostral pole of the lateral ventricle, stretching for 900–1200 μm in the caudal direction. Its rostral and caudal borders correspond approximately to +1.18 mm and +0.02 mm planes, respectively, of the Franklin and Paxinos atlas of the mouse brain.

Immunohistochemistry and double-fluorescence immunohistochemistry

One out of six 30-μm-thick coronal sections from the DG and the SVZ of animals were processed for immunohistochemistry as previously described (Bianchi et al., 2010; Contestabile et al., 2007). Immunohistochemistry was carried out on free-floating sections of the frozen brains. For BrdU immunohistochemistry, sections were denatured in 2 N HCl for 30 min at 37 °C and incubated overnight at 4 °C with a primary antibody anti-BrdU (mouse monoclonal 1:100, Roche Applied Science, Mannheim, Germany). Detection was performed with a Cy3-conjugated anti-mouse secondary antibody (dilution 1:200; Jackson Immunoresearch, West Grove, PE, USA). For Ki-67 immunohistochemistry, sections were incubated overnight at 4 °C with rabbit monoclonal anti-Ki67 antibody (1:200; Thermo Scientific Neumarkers, Fremont, CA. USA) and for 2 h with a Cy3 conjugated anti-rabbit IgG (1:200; Jackson Immunoresearch). For cleaved caspase-3 immunohistochemistry, sections were incubated overnight at 4 °C with a rabbit cleaved caspase-3 antibody (1:200; Cell Signaling Technology) and for 2 h with an HRP-conjugated anti-rabbit secondary antibody (dilution 1:200; Jackson Immunoresearch). Detection was performed using the TSA Cyanine 3 Plus Evaluation Kit (Perkin Elmer). For synaptophysin immunohistochemistry, sections from the DG were incubated for 48 h at 4 °C with mouse monoclonal anti-SYN (SY38) antibody (1:1000, MAB 5258, Millipore Bioscience Research Reagents) and for 2 h with a Cy3 conjugated anti-mouse IgG secondary antibody (1:200; Jackson Immunoresearch). For doublecortin (DCX) immunohistochemistry, sections from the DG were incubated overnight at 4 °C with a goat polyclonal anti-DCX antibody (1:100; Santa Cruz Biotechnology). Sections were then incubated for 2 h at room temperature with a biotinylated anti-goat IgG secondary antibody (1:200; Vector Laboratories) and thereafter incubated for 1 h with VECTASTAIN® ABC kit (Vector Laboratories). Detection was performed using DAB kit (Vector Laboratories). For double-fluorescence immunostaining, sections were incubated overnight at 4 °C with a primary antibody rat monoclonal anti-BrdU antibody (1:100; AbD Serotec, Kidlington, Oxford, UK) and one of the following primary antibodies: i) mouse monoclonal anti NeuN (1: 250; Chemicon, Billerica, MA, USA) and ii) mouse monoclonal anti-glial fibrillary acidic protein (GFAP) (1:400; Sigma) or with a monoclonal anti-Nestin antibody (1:200; Chemicon, Billerica, MA, USA) and

cleaved caspase-3 antibody (1:200; Cell Signaling Technology). Sections were then incubated with a Cy3 conjugated anti-rat or anti-mouse IgG (1:100; Jackson Immunoresearch) secondary fluorescent antibody, for BrdU or Nestin immunohistochemistry, respectively, a FITC conjugated anti-mouse IgG antibody (1:100; Sigma-Aldrich) for NeuN and GFAP, and a FITC conjugated anti-rabbit IgG antibody (1:100; Jackson Immunoresearch) for cleaved caspase-3 immunohistochemistry. Fluorescent images were taken with an Eclipse TE 2000-S microscope (Nikon, Tokyo, Japan) equipped with an AxioCam MRm (Zeiss, Oberkochen, Germany) digital camera or with a Leica TCS confocal microscope (Leica Microsystems, Wetzlar, Germany).

Ultra-thin consecutive sections were deparaffinized, incubated with a goat anti-DCX antibody (1:100; Santa Cruz Biotechnology) or with a rabbit cleaved caspase-3 antibody (1:200; Cell Signaling Technology). Sections were then incubated for 2 h at room temperature with a biotinylated anti-goat IgG secondary antibody (1:200; Vector Laboratories) or a biotinylated anti-rabbit IgG secondary antibody (1:200; Vector Laboratories) and thereafter incubated for 1 h with VECTASTAIN® ABC kit (Vector Laboratories). Detection was performed using DAB kit (Vector Laboratories).

Measurements

Cell counting

The total number of positive cells (BrdU, Ki-67, NeuN/BrdU, GFAP/BrdU, cleaved caspase-3, Nestin/cleaved caspase-3, DCX) was estimated by multiplying the number counted in the series of sampled sections by the inverse of the section sampling fraction (section sampling fraction = 1/6).

Stereology of the DG

In the series of Nissl-stained sections, the volume of the granule cell layer was estimated as previously described (Bianchi et al., 2010; Contestabile et al., 2007) by multiplying the sum of the cross-sectional areas by the spacing between sampled sections. Granule cell numerical density was determined using the optical fractionators (Bianchi et al., 2010). Counting frames with a side length of 30 μm and a height of 8 μm spaced in a 150 μm square grid (fractionator) were systematically used. The total number of granule cells was estimated as the product of the volume of the granule cell layer and the numerical density.

Measurement of the dendritic tree

Dendritic trees of DCX positive granule cells of the DG were traced with a dedicated software, custom-designed for dendritic reconstruction (Immagini Computer, Milan, Italy), interfaced with Image Pro Plus (Media Cybernetics, Silver Spring, MD, USA). The dendritic tree was traced live, at a final magnification of 500×, by focusing into the depth of the section. The operator starts with branches emerging from the cell soma and after having drawn the first parent branch goes on with all daughter branches of the next order in a centrifugal direction. At the end of tracing the program reconstructs the number and length of individual branches, the mean length of branches of each order and total dendritic length.

Connectivity in the molecular layer of the DG

To evaluate the connectivity in the molecular layer of the DG, intensity of SYN immunoreactivity (IR) was determined by optical densitometry of immunohistochemically-stained sections. Fluorescence images were captured using a Nikon Eclipse E600 microscope equipped with a Nikon Digital Camera DXM1200 (ATI system). Densitometric analysis of SYN in the inner (I), middle (M) and outer (O) third of the molecular layer was carried out using Nis-Elements Software 3.21.03 (Nikon). For each image, the intensity threshold was estimated by analyzing the distribution of pixel intensities in the image areas that did not contain IR. This value was then subtracted to calculate the IR of each sampled area.

Western blotting

The following antibodies were used: anti-GAPDH (1:5000) and anti-CDKL5 (1:500) (Sigma); anti-phosphorylated Erk1/2 (1:1000), anti Erk1/2 (1:1000), anti-phospho-AKT-Ser^{473} (1:1000), anti-phospho-AKT-Thr^{308} (1:1000), anti-AKT (1:1000), anti-phospho-GSK-3β-Ser^{9} (1:1000), anti-GSK-3β (1:1000), anti-phospho-CRMP2-Thr^{514} (1:1000) and anti-CRMP2 (1:1000) (Cell Signaling Technology); anti β-catenin (1:1000; BD Transduction Laboratories); anti-phospho-CREB-Ser^{133} (1:1000) and anti-CREB (1:1000) (Upstate Biotechnology). For the preparation of total cell extracts, cells were lysed in RIPA buffer (Tris–HCl 50 mM, NaCl 150 mM, Triton X-100 1%, sodium deoxycholate 0.5%, SDS 0.1%, protease and phosphatase inhibitors cocktails 1%; Sigma). For the preparation of tissue extracts, the hippocampi from P19 mice were homogenized in RIPA buffer. Extracts were immediately processed by Western blot or kept frozen (−80 °C) until assayed. Sample protein concentration was estimated using the Lowry method (Lowry et al., 1951). Equivalent amounts (50 μg) of protein were subjected to electrophoresis on a 10% SDS-polyacrylamide gel. Densitometric analysis of digitized images was performed using Scion Image software (Scion Corporation, Frederick, MD, USA) and intensity for each band was normalized to the intensity of the respective total protein levels or GAPDH band.

Y-maze test

Y-Maze Spontaneous Alternation was used to measure the willingness of mice to explore new environments and hippocampus-dependent spatial reference memory. This test was administered at 2 months of age. Each mouse was placed at the distal part of one arm facing the center of the maze. Each of the three arms was 34 cm × 5 cm × 10 cm height, angled 120° from the others and made of gray opaque plastic. After introduction into the maze, the animal is allowed to freely explore the three arms for 8 min. Over the course of multiple entries into the arm, the subject should show a tendency to enter a less recently-visited arm. Arm entries were defined by the presence of all four paws in an arm. The 8-min trial was recorded and scored via the ANY-maze videotracking software (Stoelting). The maze was cleaned with 50% ethanol after each trial. The percentage of spontaneous alternations is defined as: (total alternations/total arm entries − 2) × 100. One alternation is defined as consecutive entries into three different arms. Because of the novelty of the animal model, and in order to avoid biases related to the procedure of animal selection, we decided that all the animals generated in the lab in one breeding session would be included for behavioral testing. This explains the unequal group number composition. Bartlett's test for equal variances gave negative results, thus indicating that the unequal group composition did not affect the ANOVA analysis of Y-maze data. Finally, animals that had not completed at least 10 entries were excluded from analysis. This led to the exclusion of six animals, equally distributed among the different genotypes.

NPC cultures and treatments

Cells were isolated from the subventricular zone (SVZ) of newborn (P1–P2) Cdkl5 KO +/+, Cdkl5 KO −/− and Cdkl5 KO +/− female mice. To obtain neurospheres, cells were cultured in suspension in DMEM/F12 (1:1) containing B27 supplements (2%), FGF-2 (20 ng/ml), EGF (20 ng/ml), heparin (5 μg/ml), penicillin (100 units/ml), and antibiotics, as previously reported (Trazzi et al., 2011). Primary neurospheres were dissociated at days 7–8 using Accutase (PAA, Pasching, Austria) to derive secondary neurospheres. The subculturing protocol consisted of neurosphere passaging every 7 days with whole culture media change (with freshly added FGF-2 and EGF). All experiments were done using neurospheres obtained after one to three passages from the initially prepared cultures. Cell cultures

were kept in a 5% CO_2 humidified atmosphere at 37 °C. Lithium chloride (2 mM; Sigma) was administrated on alternate days.

Viral particles transduction

NPCs were infected, at day 1 post-plating, with CDKL5 adenovirus particles (Vector BioLabs) or GFP adenovirus particles (Vector BioLabs) at 100 multiplicities of infection (MOI).

BrdU immunocytochemistry

For proliferation analysis dissociated neurospheres were cultured for 3 days, treated with 10 μM BrdU for an additional 16 h and harvested onto microscope slides by cytospin centrifugation (215 × g, 5 min, Shandon, Thermo, Dreieich, Germany). Specimens, processed as previously described (Contestabile et al., 2009), were incubated with a mouse anti-5-bromo-2-deoxyuridine (BrdU) monoclonal antibody (1:100; Roche Applied Science) and a Cy3-conjugated anti-mouse secondary antibody (1:200; Sigma). Samples were counterstained with Hoechst-33258.

In vitro differentiation, immunocytochemistry and analysis of neurite length

Neurospheres were dissociated into a single cell suspension and plated onto poly-L-ornithyine-coated 24-well chamber slides at a density of 3×10^4 cells per well. Cells were cultured for 2 days in a DMEM/F12 medium containing EGF (20 ng/ml), FGF (20 ng/ml) and 2% fetal bovine serum (FBS), and then transferred to a differentiation medium (EGF and FGF free plus 1% FBS) for 6 or 12 days. Every 2 days, half of the medium was replaced with fresh differentiation medium. For immunofluorescent staining, differentiated NPC cultures were paraformaldehyde-fixed and stained with antibodies against: GFAP (1:400; Sigma) and β-tubulin III (1:100; Sigma) as primary antibodies, and with mouse FITC-conjugated (1:200; Sigma) and rabbit Cy3-conjugated (1:200; Jackson Laboratories), as secondary antibodies. Samples were counterstained with Hoechst-33258. Ten random fields from each coverslip were photographed and counted. The number of positive cells for each marker referred to the total number of Hoechst-stained nuclei. Evaluation of neurite length was performed by using the image analysis system Image Pro Plus (Media Cybernetics, Silver Spring, MD, USA). The average neurite length per cell was calculated by dividing the total neurite length by the number of cells counted in the areas.

Statistical analysis

Data are expressed as mean ± SE, and statistical significance was assessed by a two-way analysis of variance (ANOVA), followed by Bonferroni's *post hoc* test, Dunnet's test or by the two-tailed t-test. Significance was set to $p \leq 0.05$. Statistical analysis was performed using GraphPad Prism 4.0.

Results

Loss of Cdkl5 increases proliferation rate in the dentate gyrus

In order to establish whether lack of Cdkl5 affects progenitor cell proliferation in the hippocampal dentate gyrus (DG), wild type and Cdkl5 KO mice aged 40 days (P40) were injected for five consecutive days with BrdU and sacrificed 24 h after the last BrdU injection. Since Cdkl5 is localized on the X chromosome, the genotypes deriving from inactivation of the Cdkl5 gene are: homozygous females (Cdkl5 −/−), heterozygous females (Cdkl5 +/−) and hemizygous males (Cdkl5 −/Y). Observation of images from wild type (Cdkl5 +/+) and Cdkl5 −/− females showed that KO females had more BrdU positive cells than their wild type littermates (Fig. 1A). A quantitative analysis revealed that the number of BrdU positive cells was higher in both Cdkl5 −/− and Cdkl5 −/Y (+20 ± 1.7% and +23 ± 2.1%, respectively; $p < 0.01$ Bonferroni's test after ANOVA) compared to wild type mice (Fig. 1B). The number of BrdU positive cells in Cdkl5 +/− mice showed a slight but not significant increase in comparison with wild type females (Fig. 1B), which may be consistent with a mosaic of knockout and wild type cells as a result of X-inactivation (Goto and Monk, 1998). Similar results were obtained with immunohistochemistry for Ki-67, an endogenous marker of actively proliferating cells (Fig. 1C, D). The increased proliferative ability of neuronal precursor cells due to the lack of Cdkl5 expression suggests that this gene exerts a negative role on cell proliferation.

Loss of Cdkl5 reduces the survival rate of newborn cells in the dentate gyrus

In order to evaluate the survival rate of the newborn cells, we counted the number of BrdU positive cells present in the DG 30 days after BrdU administration, in mice aged 75 days (P75). Most of the surviving cells were located in the granule cell layer, the final destination of new granule neurons. We found that both Cdkl5 −/− and Cdkl5 −/Y mice had the same number of BrdU labeled cells as wild type mice (Fig. 2A). This suggests that the surplus of cells born at P45 in Cdkl5 −/− and Cdkl5 −/Y mice was offset by a reduction in the survival rate. The ratio between the number of BrdU positive cells present in the DG at 1 month (Fig. 2A) and 2 h (Fig. 1B) after the last BrdU injection provides an estimate of the net survival rate. We found that in wild type mice 50% of the cells born at P45 survived, whereas in Cdkl5 −/− mice 39 ± 1.2% of the original cells survived ($p < 0.01$ Bonferroni's test after ANOVA) and in Cdkl5 −/Y mice 43 ± 1.9% survived ($p < 0.01$ Bonferroni's test after ANOVA). A significant difference in cell survival rate was also found in Cdkl5 +/− compared to wild type mice (45 ± 1.7 %; $p < 0.01$ Bonferroni's test after ANOVA).

In an attempt to examine whether a lack of Cdkl5 triggers apoptotic cell death we evaluated the number of apoptotic cells in the DG by counting the number of cells that expressed cleaved caspase-3 (Fig. 2B). Most of the apoptotic cells were in the innermost portion of the granule cell layer. We observed an increase in cell death in both Cdkl5 −/− and Cdkl5 −/Y mice (+40 ± 3.4% and +32 ± 2.9%, respectively; $p < 0.001$ Bonferroni's test after ANOVA; Fig. 2B) compared to wild type mice and a less pronounced but significant increase in Cdkl5 +/− mice (+14 ± 1.9; $p < 0.01$ Bonferroni's test after ANOVA; Fig. 2B). This evidence suggests that a lack of Cdkl5 decreases the survival rate of newborn cells in Cdkl5 KO mice.

Loss of Cdkl5 specifically decreases survival of postmitotic neurons

We examined the phenotype of the surviving cells 30 days after BrdU administration through immunofluorescent double-labeling for BrdU and either a neuronal marker (NeuN) or an astrocytic marker (GFAP). Both Cdkl5 −/− and Cdkl5 −/Y mice had fewer (−20 ± 2.0% and −30 ± 2.5%, respectively; $p < 0.001$ and $p < 0.01$, Bonferroni's test after ANOVA) new neurons (NeuN/BrdU positive cells; Fig. 3A, B) in comparison with wild type mice, a similar number of new astrocytes (GFAP/BrdU positive cells; Fig. 3A, B) and a larger number of cells with an undetermined phenotype (+190 ± 12% and +300 ± 27%, respectively; $p < 0.001$ and $p < 0.01$, Bonferroni's test after ANOVA; other; Fig. 3A, B). A similar effect was also found in Cdkl5 +/− mice (Fig. 3A). These data show that the lack of Cdkl5 dampens the formation of new granule neurons without affecting astrogliogenesis.

In the course of adult hippocampal neurogenesis, new cells within the subgranular zone (SGZ) of the DG go through a series of stages associated with proliferative activity, from the stem cell stage (type 1) to the intermediate progenitor stages (type 2/3), and onto postmitotic maturation (Kempermann et al., 2004) (Fig. 4A). Doublecortin (DCX) is widely expressed by the actively dividing type 2b and type 3 intermediate progenitor cells and by immature granule neurons (Fig. 4A). To determine whether the loss of Cdkl5 specifically affects a particular stage of granule cell formation, we labeled brain sections of wild type and Cdkl5 KO mice with DCX. As shown in Fig. 4B, DCX positive cells were

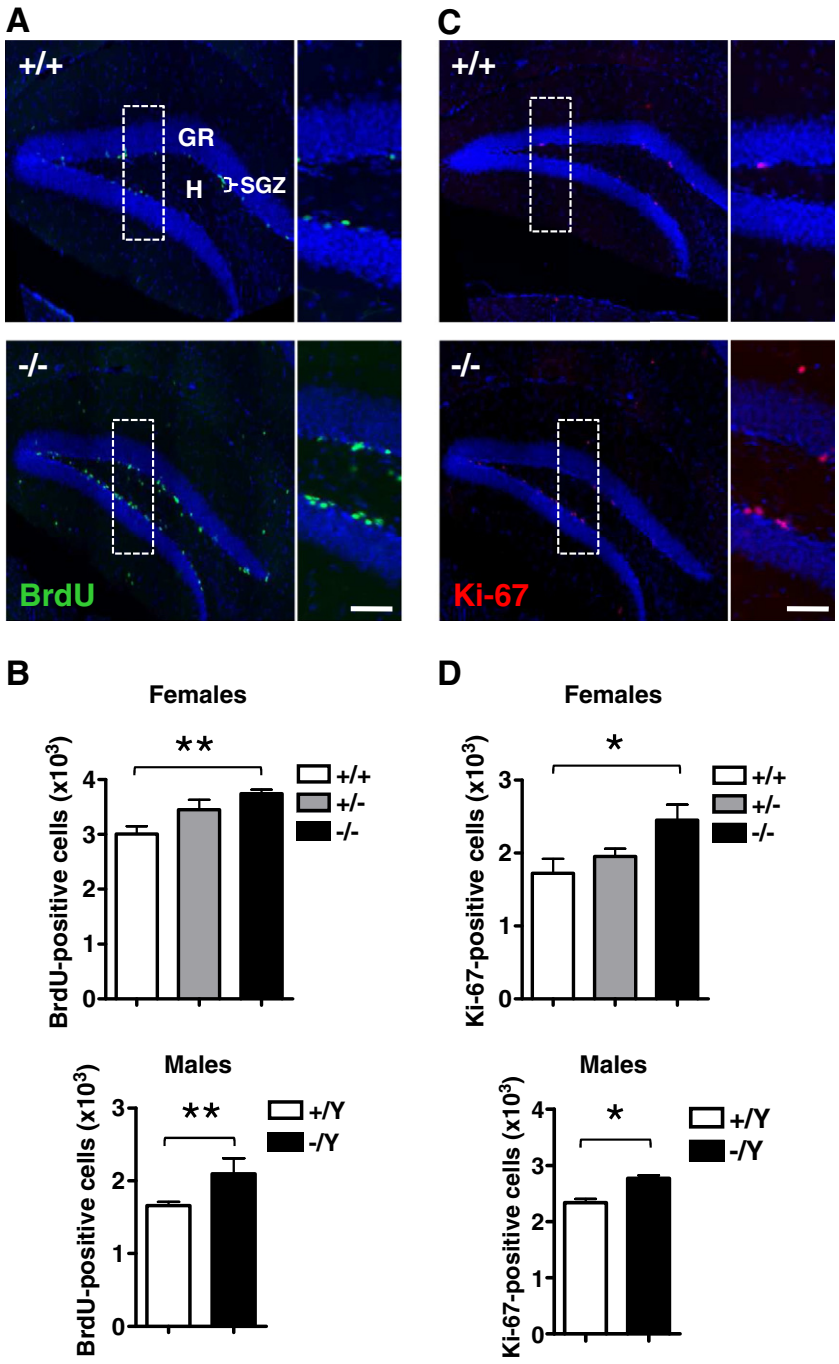

Fig. 1. Neuronal precursor proliferation in the dentate gyrus of Cdkl5 KO mice. A, B: Animals were injected with BrdU for five consecutive days and sacrificed 24 h after the last BrdU injection on P45. Examples of sections processed for fluorescent immunostaining for BrdU from the dentate gyrus (DG) of wild type (+/+) and homozygous (−/−) Cdkl5 KO female mice (A). Scale bars = 200 μm (lower magnification) and 80 μm (higher magnification). The dotted boxes indicate the regions shown at a higher magnification. Number of BrdU positive cells in the granule cell layer (GR) plus subgranular zone (SGZ) plus hilus (H) of homozygous (−/−; n = 6), heterozygous (+/−; n = 6) and wild type (+/+; n = 5) Cdkl5 KO female mice and hemizygous (−/Y; n = 6) and wild type (+/Y; n = 6) Cdkl5 KO male mice (B). C: Examples of sections processed for fluorescent immunostaining for Ki-67 from the DG of wild type (+/+) and homozygous (−/−) Cdkl5 KO female mice. Scale bars = 200 μm (lower magnification) and 80 μm (higher magnification). D: Number of Ki-67 positive cells in the GR + SGZ + H of the same animals as in B. Values in B to D represent totals for one DG (mean ± SD). (*)$p < 0.07$; *$p < 0.05$; **$p < 0.01$ (Bonferroni's test after ANOVA).

present in the SGZ and deepest portion of the granule cell layer (Fig. 4B). While the orientation of type 2b/3 cells is parallel to the SGZ (Fig. 4A, B; asterisks), immature granule neurons have a vertical orientation and extend long apical processes into the granule cell layer (Fig. 4A, B; arrows). Based on these features, it was possible to divide DCX positive cells into two stages of development: type 2b/3 cells and immature neurons. We found that Cdkl5 KO mice had more 2b/3 type cells in comparison with wild type mice but a reduced number of immature neurons (Fig. 4C). These data indicate that the lack of Cdkl5 affects type 2b/3 cells (mitotic cells) and differentiating (postmitotic) neurons in an opposite manner. This is consistent with the increased number of undifferentiated cells (other) and the reduced number of cells differentiated into neurons (NeuN/BrdU positive cells) found in Cdkl5 KO mice (see Fig. 3A, B). In order to establish whether the reduced number of immature neurons in KO mice was due to an increase in cell death, we evaluated the number of cells that were positive for both DCX and cleaved caspase-3. We found that Cdkl5 KO mice showed a notably higher number of DCX/cleaved caspase-3 positive immature neurons in comparison

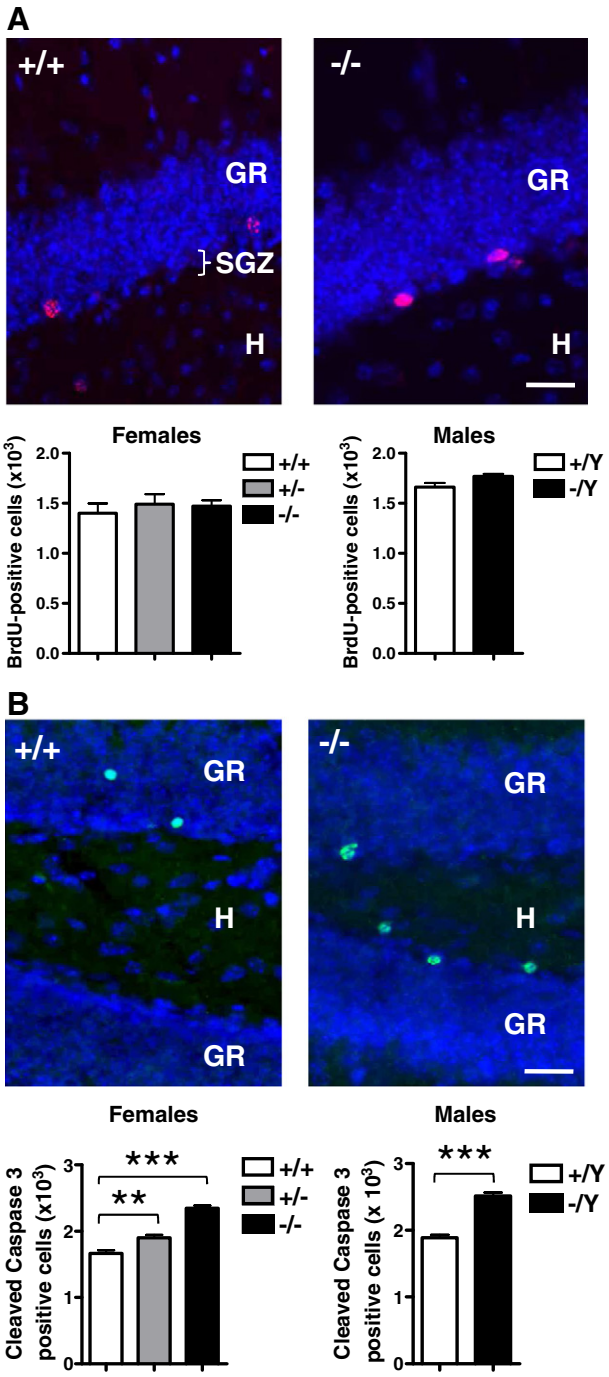

Fig. 2. Survival of neuronal precursors in the dentate gyrus of Cdkl5 KO mice. A: Examples of sections processed for fluorescent immunostaining for BrdU from the dentate gyrus (DG) of wild type (+/+) and homozygous (−/−) Cdkl5 KO female mice (upper panels). These animals were injected with BrdU for five consecutive days and sacrificed 1 month after the last BrdU injection (on P75). Scale bar = 50 μm. Number of BrdU positive cells in the granule cell layer (GR) plus subgranular zone (SGZ) plus hilus (H) of homozygous (−/−; n = 5), heterozygous (+/−; n = 4) and wild type (+/+; n = 4) Cdkl5 KO female mice and hemizygous (−/Y; n = 4) and wild type (+/Y; n = 4) Cdkl5 KO male mice. B: Examples of sections processed for fluorescent immunostaining for cleaved caspase-3 from the DG of wild type (+/+) and homozygous (−/−) Cdkl5 KO female mice. Scale bars = 40 μm. Number of caspase-3 positive cells in the GR + SGZ + H of homozygous (−/−; n = 6), heterozygous (+/−; n = 6) and wild type (+/+; n = 6) Cdkl5 KO female mice and hemizygous (−/Y; n = 6) and wild type (+/Y; n = 5). Values in A and B represent totals for one DG (mean ± SD). **p < 0.01; ***p < 0.001 (Bonferroni's test after ANOVA).

with wild type mice (Fig. 4D, E), with no difference in the number of DCX/caspase-3 positive 2b/3 type cells (Fig. 4D, E). To establish whether nestin-positive primary progenitor cells (type 1) and intermediate progenitor cells (type 2a) (Fig. 4A) also exhibit an increase in apoptotic cell death, we evaluated the number of cells that were positive for both nestin and cleaved caspase-3. We found that Cdkl5 KO mice showed no difference in the number of nestin/caspase-3 positive 1/2a type cells in comparison with wild type mice (Supplementary Fig. 1). This evidence suggests that the reduced number of new neurons in Cdkl5 KO mice (see Figs. 3 and 4C) is due to an increase in cell death that specifically affects early postmitotic neurons.

Loss of Cdkl5 results in a reduced net number of granule cells in the dentate gyrus

To establish the impact of the reduction in the number of newly-formed granule neurons in Cdkl5 KO mice on the overall granule cell number, we stereologically evaluated the total granule cell number in mice aged 45 and 75 days. We found no difference between Cdkl5 KO and wild type mice in the volume of the granule cell layer (Fig. 5B), but a reduced granule cell density (Fig. 5C) and a reduced number of granule cells (Fig. 5D) was present in P45 Cdkl5 KO compared to wild type mice. The reduction in cell number was −12 ± 1.2% and −10 ± 0.5%, respectively, in Cdkl5 −/− and Cdkl5 −/Y mice, and −8 ± 0.7% in Cdkl5 +/− mice ($p < 0.001$ and $p < 0.01$, Bonferroni's test after ANOVA; Fig. 5D). Similar results were obtained in P75 Cdkl5 KO mice (data not shown). Consistently with the higher apoptotic cell death in Cdkl5 KO mice estimated by cleaved caspase-3 immunostaining (Fig. 2B), we noted a higher number of pyknotic nuclei in the innermost granule cell layer of Cdkl5 KO mice, indicating a larger number of dying cells (Fig. 5A, arrowheads).

Loss of Cdkl5 results in dendritic hypotrophy of newborn granule cells

Dendritic arborization is significantly reduced in the cortical pyramidal neurons of Cdkl5 KO mice compared to their wild type counterparts (Amendola et al., 2014). The dendritic morphology of newborn granule cells can be analyzed through immunohistochemistry for DCX, taking advantage of the expression of this protein in the cytoplasm of immature neurons during the period of neurite elongation (from 1 to 4 weeks after neuron birth). In order to establish the effect of Cdkl5 loss on the dendritic development of newborn granule cells, we examined the dendritic morphology of DCX positive cells. Fig. 4B clearly shows that DCX positive neurons of Cdkl5 KO mice had fewer processes than those of their wild type counterparts. Quantification of the dendritic size of DCX positive cells showed that Cdkl5 −/− and Cdkl5 −/Y mice had a shorter dendritic length (−44 ± 5% and −34 ± 7%, respectively, $p < 0.01$, Bonferroni's test after ANOVA; Fig. 6A) and a reduced number of segments (−46 ± 2% and −36 ± 9%, respectively, $p < 0.05$, Bonferroni's test after ANOVA; Fig. 6B) than wild type mice. The reduction in dendritic length and number of segments in Cdkl5 +/− mice (−41 ± 6% and −45 ± 4%, respectively; $p < 0.01$ and $p < 0.05$ Bonferroni's test after ANOVA; Fig. 6A, B) was very similar to that found in Cdkl5 −/− mice.

To dissect the effects of CDKL5 loss on the details of dendritic architecture, we examined each dendritic order separately. A striking feature of Cdkl5 KO mice was the absence of branches of higher order. While wild type female mice had up to nine orders of branches, Cdkl5 −/− and Cdkl5 +/− mice lacked branches of orders 7–9 (Fig. 6C, arrows). In addition, Cdkl5 −/− and Cdkl5 +/− mice showed a reduced branch length of orders 4–7 (Fig. 6C) and a reduced number of branches of orders 5 and 6 (Fig. 6D). Altogether, similar alterations were found when comparing Cdkl5 −/Y and wild type mice (Fig. 6C, D). Taken together, these data indicate that in Cdkl5 KO mice the dendritic tree of the newborn granule cells is hypotrophic and that this defect is due to a reduction in the number and length of branches of intermediate order and a lack of branches of higher order.

It is likely that a reduction in connectivity is the counterpart of the dendritic hypotrophy that characterizes the newborn granule cells of

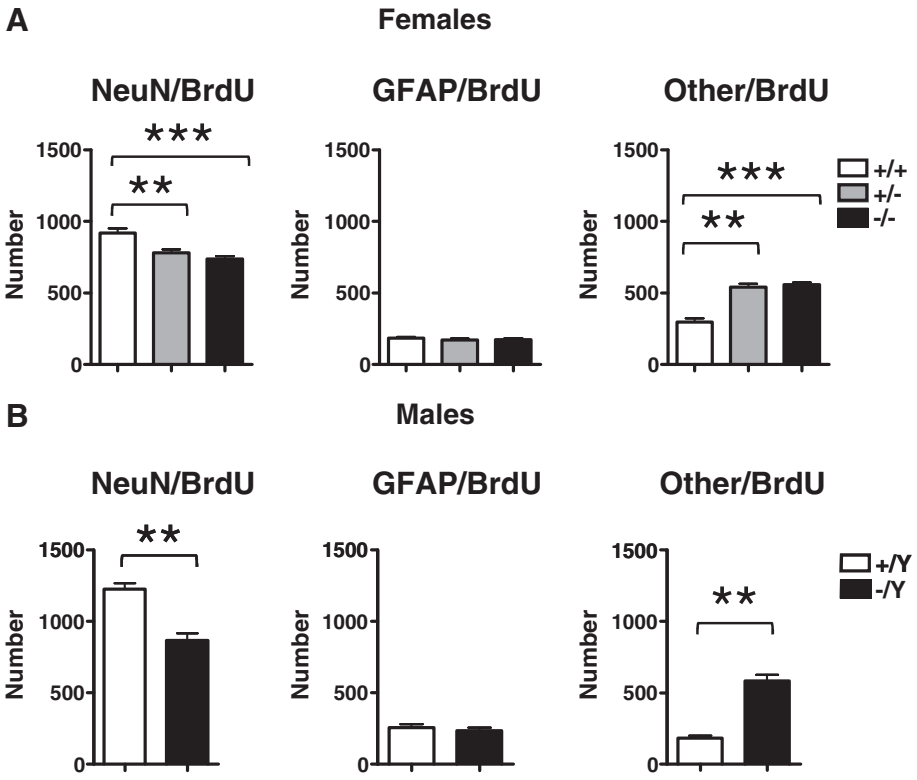

Fig. 3. Phenotype of the surviving cells in the dentate gyrus of Cdkl5 KO mice. A, B: Absolute number of surviving cells with a neuronal phenotype (NeuN/BrdU), an astrocytic phenotype (GFAP/BrdU) and an undetermined phenotype (Other; NeuN −/GFAP −/Brdu + cells) in the dentate gyrus (DG) of homozygous (−/−; n = 4), heterozygous (+/−; n = 4) and wild type (+/+; n = 4) Cdkl5 KO female mice (A) and hemizygous (−/Y; n = 4) and wild type (+/Y; n = 4) Cdkl5 KO male mice (B). These animals were injected for five consecutive days with BrdU and sacrificed 1 month after the last BrdU injection (on P75). Values in A and B represent totals for one DG (mean ± SD). **p < 0.01; ***p < 0.001 (Bonferroni's after ANOVA).

Cdkl5 KO mice. Synaptophysin (SYN; also known as p38) is a synaptic vesicle glycoprotein that is a specific marker of presynaptic terminals. We found that in Cdkl5 KO mice the optical density of SYN was significantly lower than in wild type mice in the outer (O), middle (M) and inner (I) molecular layer (Fig. 6E, F), suggesting that Cdkl5 KO mice had fewer synaptic contacts in the DG.

Loss of Cdkl5 increases proliferation rate and apoptotic cell death in the SVZ

We examined the effect of Cdkl5 loss in the SVZ, a region that, similar to the SGZ of the DG, retains a neurogenic potential in the adult brain. Observation of images from the SVZ of Cdkl5 KO and wild type mice clearly showed that Cdkl5 KO mice had more Ki-67 positive cells (Supplementary Fig. 2A). Quantification of the number of Ki-67 positive cells showed that both Cdkl5 −/− and Cdkl5 −/Y mice had more Ki-67 positive cells (+30 ± 5% and +20 ± 3.9%, respectively; $p < 0.01$ and $p < 0.05$, Bonferroni's test after ANOVA; Supplementary Fig. 2B) compared to wild type mice. A less pronounced but significant disparity in the number of proliferating cells was found in Cdkl5 +/− mice compared to wild type mice (+14 ± 3.7%, $p < 0.05$ Bonferroni's test after ANOVA; Supplementary Fig. 2B). Evaluation of the total number of apoptotic cells, showed that in the SVZ of Cdkl5 −/−, Cdkl5 +/− and Cdkl5 −/Y mice there were more apoptotic cells (+21 ± 2.7%, +15 ± 2.4%, +21 ± 3.9%, respectively; $p < 0.01$ and $p < 0.05$, Bonferroni's test after ANOVA; Supplementary Fig. 2C, D) than in their wild type counterparts.

Alterations in the AKT/GSK-3β pathway are involved in neurogenesis and neuronal maturation defects in Cdkl5 KO mice

Glycogen synthase kinase 3 (GSK-3β) is a ubiquitously active serine/threonine kinase which is inhibited upon phosphorylation at Ser9 by activated protein kinase B (PKB/AKT). GSK-3β (dephosphorylated at Ser9) is a crucial inhibitory regulator of many neuronal functions, including neurite outgrowth, synapse formation, neurogenesis and survival of newly-generated neurons (Cole, 2012). The AKT/GSK-3β pathway exerts its functions by modulating the activity of a wide range of substrates (Cole, 2012). An outline of key elements of this pathway is reported in Fig. 7A. We and others had previously shown the disruption of AKT/mTOR/S6 signaling in Cdkl5 KO mice (Amendola et al., 2014; Wang et al., 2012) (diagram in Fig. 7A). In the current study we were interested in establishing whether the AKT/GSK-3β pathway is also deregulated in Cdkl5 KO mice. Evaluation of the phosphorylation levels of the AKT/GSK-3β pathway showed lower phosphorylation levels of: i) PDK1 (PDK1 stands at the head of the AKT/GSK-3β pathway by phosphorylating AKT), ii) AKT, at its two critical residues namely Thr308 and Ser473, iii) GSK-3β at Ser9 (its inhibitory site), and iv) CREB at Ser133 in Cdkl5 KO in comparison with wild type mice (Fig. 7B, C). While CREB phosphorylation and consequent DNA binding is inhibited by activated (Ser9 dephosphorylated) GSK-3β (diagram in Supplementary Fig. 3) (Grimes and Jope, 2001), collapsin response mediator protein-2 (CRMP-2) is phosphorylated and consequently inactivated by GSK-3β (Supplementary Fig. 3) (Yoshimura et al., 2005). In contrast, GSK-3β controls the amount of β-catenin by negatively regulating β-catenin protein stability (Supplementary Fig. 3) (Wada, 2009). In line with an increased activity of GSK-3β, we found higher phosphorylation levels of CRMP2 and lower levels of β-catenin (Fig. 7B, C). No differences were found between Cdkl5 KO and wild type mice in the phosphorylation levels of ERK (Fig. 7B, C), suggesting a specific alteration of the AKT/GSK-3β pathway in the absence of Cdkl5.

This evidence suggests that alteration of the AKT/GSK-3β pathway may underlie the developmental defects due to loss of CDKL5. In order to clarify this issue, we used cultures of neuronal precursor cells (NPCs) from Cdkl5 KO mice. We first sought to establish

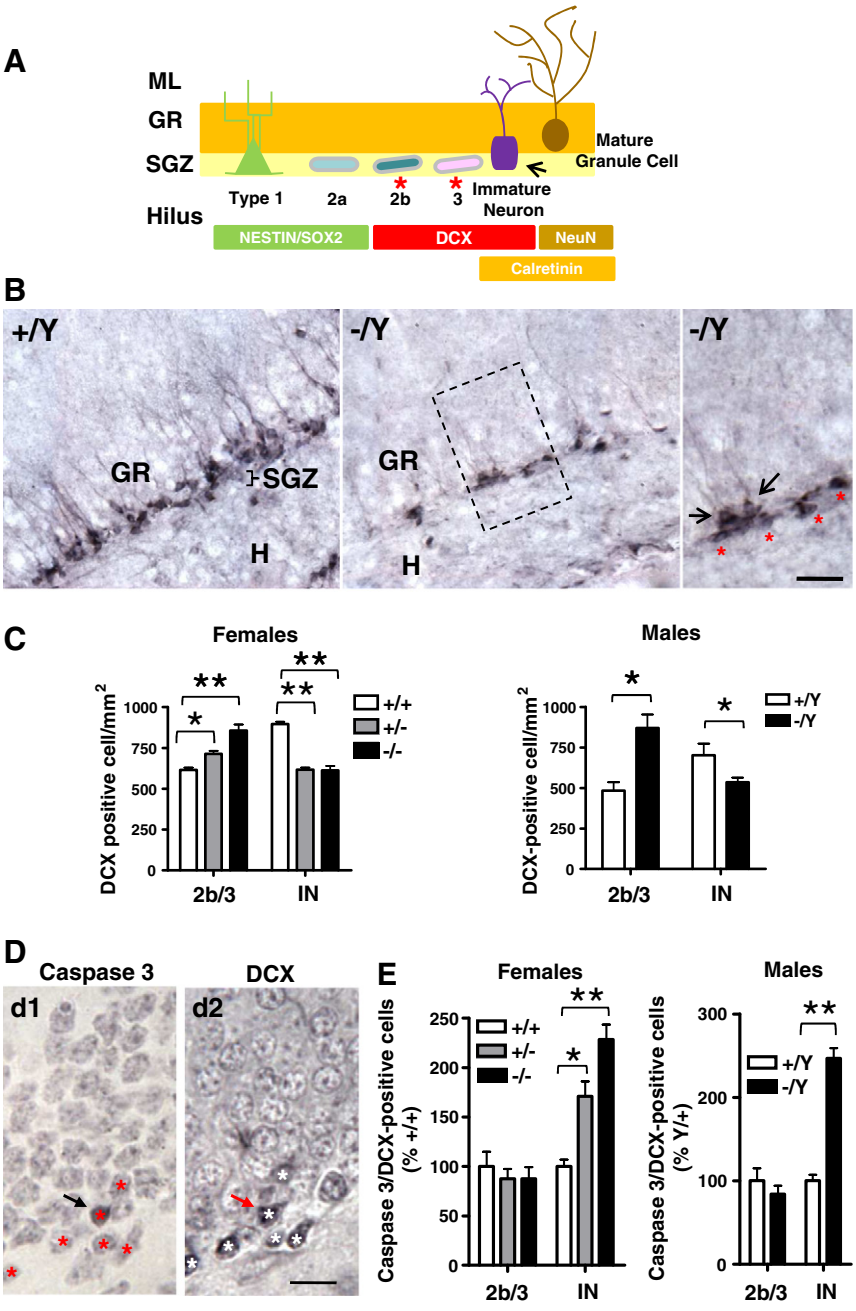

Fig. 4. Survival of postmitotic neurons in the dentate gyrus of Cdkl5 KO mice. A: Diagram of hippocampal neurogenesis. During the mitotic phase, two types of progenitors proliferate in the subgranular zone (SGZ) of the dentate gyrus (DG): primary progenitor cells (type 1 cells, expressing Nestin and Sox2) and intermediate progenitor cells (type 2a/b and type 3 cells). Before becoming postmitotic, type 2b and type 3 intermediate progenitors commit to a neuronal fate and begin expressing DCX. In the postmitotic phase, DCX positive newborn neurons derived from type 3 cells undergo a morphological and physiological maturing process with the sequential expression of calretinin and NeuN upon final maturation. B: Examples of sections processed for DCX immunostaining from the DG of wild type (+/Y) and hemizygous (−/Y) Cdkl5 KO male mice. The high magnification photomicrograph (panel on the right) shows immature DXC positive neurons (vertical orientation with apical processes; black arrows) in the innermost portion of the granule cell layer (GR) and type 2b/3 DCX positive precursor cells (orientation parallel to the GR; red asterisks) in the subgranular zone (SGZ). The dotted box indicates the region shown at a higher magnification on the right. Scale bars = 60 μm (lower magnification images) and 15 μm (higher magnification image). C: Number of DCX positive cells in the DG of homozygous (−/−; n = 5), heterozygous (+/−; n = 4) and wild type (+/+; n = 4) Cdkl5 KO female mice and hemizygous (−/Y; n = 4) and wild type (+/Y; n = 4) Cdkl5 KO male mice. Type 2b/3 (2b/3) cells and immature neurons (IN) were counted separately. Data are expressed as number of cells/mm^2. D: Examples of cleaved caspase-3 positive cells (d1, black arrow) and DCX positive cells (d2, white asterisks) detected in ultra thin adjacent sections processed for immunostaining for cleaved caspase-3 or DCX, from the DG of a wild type (+/+) female mouse. Computer-based image overlay of two adjacent ultra thin sections immunostained for either cleaved caspase-3 or DCX allowed us to identify the same cells. The red asterisks in d1 indicate cells corresponding to the DCX positive cells, identified in the section in d2. Likewise, the red arrow in d2 indicates the cleaved caspase positive cell identified in d1. Scale bars = 15 μm. E: Number of cleaved caspase-3/DCX positive cells, identified as shown in D, in the DG of homozygous (−/−; n = 4), heterozygous (+/−; n = 3) and wild type (+/+; n = 3) Cdkl5 KO female mice and hemizygous (−/Y; n = 4) and wild type (+/Y; n = 3) Cdkl5 KO male mice. Type 2b/3 cells (2b/3) and immature neurons (IN) were counted separately. Data are expressed as percentages in comparison with wild type mice. Values in C and E are mean ± SD. *$p < 0.05$; **$p < 0.01$ (Bonferroni's test after ANOVA).

whether cultures of NPCs exhibit the same defects observed *in vivo*. Neurospheres derived from the SVZ of homozygous (−/−) Cdkl5 KO females exhibited a higher proliferation rate compared to those of their wild type counterparts (+15 ± 1.9%, $p < 0.01$ Bonferroni's test after ANOVA; Fig. 8A). No difference in apoptotic cell death was observed between wild type and Cdkl5 KO neurospheres, as estimated through cleaved caspase-3 immunostaining (Fig. 8B) and the pyknotic appearance of the nuclei of dying cells (data not shown). This confirms

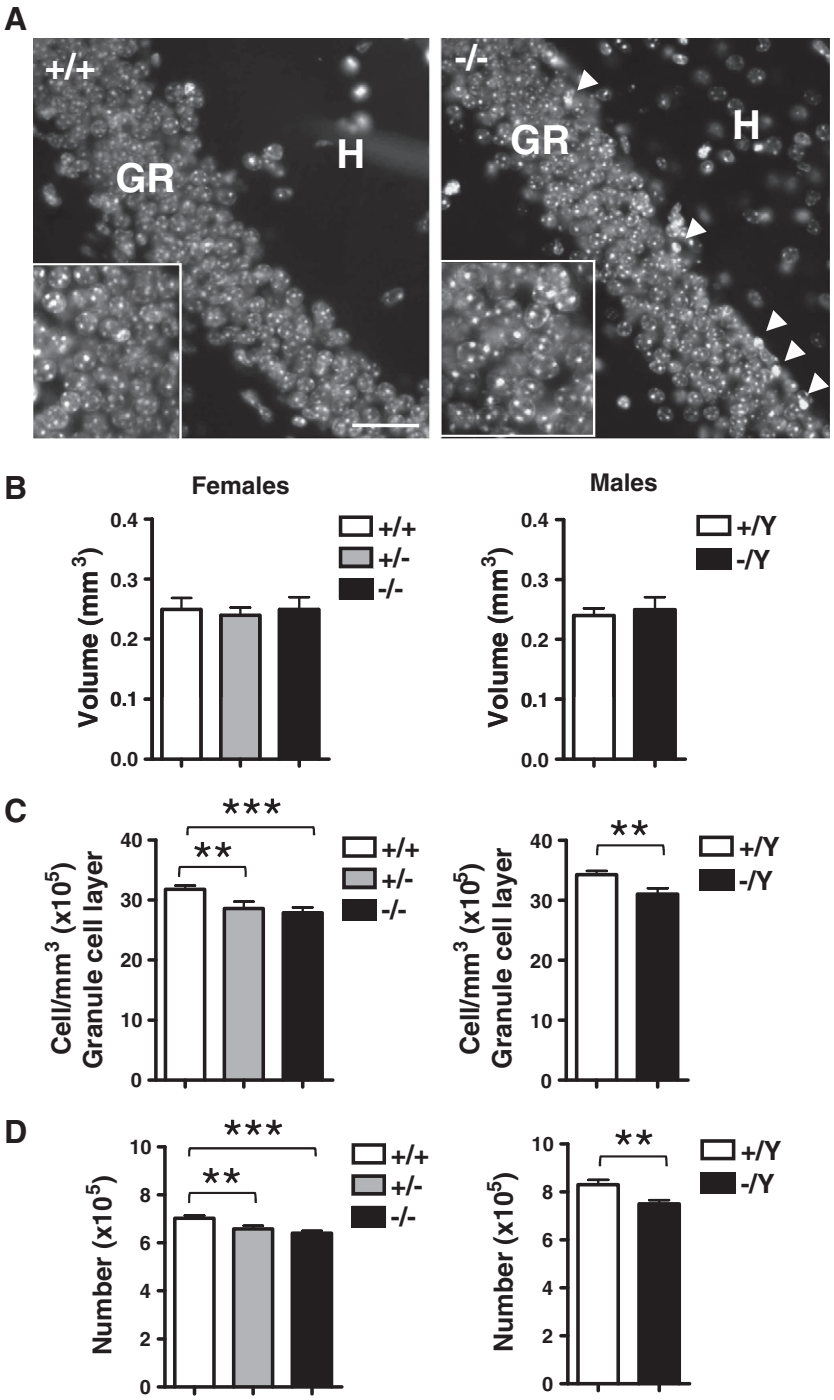

Fig. 5. Stereology of the dentate gyrus of Cdkl5 KO mice. A: Examples of Hoechst-stained sections from the dentate gyrus of wild type (+/+) and homozygous (−/−) Cdkl5 KO female mice. The white arrowheads indicate pyknotic cells. Scale bar = 80 μm (lower magnification) and 20 μm (higher magnification). B–D: Volume of the granule cell layer (B), density of granule cells (C) and total number of granule cells (D) in homozygous (−/−; n = 6), heterozygous (+/−; n = 6) and wild type (+/+; n = 6) Cdkl5 KO female mice and hemizygous (−/Y; n = 6) and wild type (+/Y; n = 6) Cdkl5 KO male mice aged 45 days. Values (mean ± SD) refer to one dentate gyrus. **p < 0.01; ***p < 0.001 (Bonferroni's test after ANOVA). Abbreviations: GR, granule cell layer; H, hilus.

that loss of Cdkl5 does not induce an increase in cell death during the stage of proliferation of NPCs. In order to determine the effect of Cdkl5 loss on cell death in post-mitotic NPCs, we evaluated the number of cleaved caspase-3 positive cells after 1 day in differentiating culture conditions. We found that cultures of differentiating NPCs from (−/−) female Cdkl5 KO mice exhibited a notably higher number of caspase-3 positive cells in comparison with their wild type counterparts (+350 ± 17%, $p < 0.001$, Bonferroni's test after ANOVA; Fig. 8C), confirming that a loss of Cdkl5 is accompanied by an increase in cell death during the stage of differentiation. A significant difference in cell survival rate was also found in NPCs from heterozygous (+/−) female Cdkl5 KO mice (187 ± 21.4 %; $p < 0.01$ Bonferroni's test after ANOVA; data not shown), which may be consistent with a mosaic of knockout and wild type cells. Evaluation of the number of new neurons (β-tubulin III positive cells) and new astrocytes (GFAP positive cells) after 7 days of differentiation showed that in differentiated cultures of Cdkl5 −/− NPCs the number of neurons was remarkably smaller compared to wild type NPCs (−82 ± 7%, $p < 0.001$, Bonferroni's test after

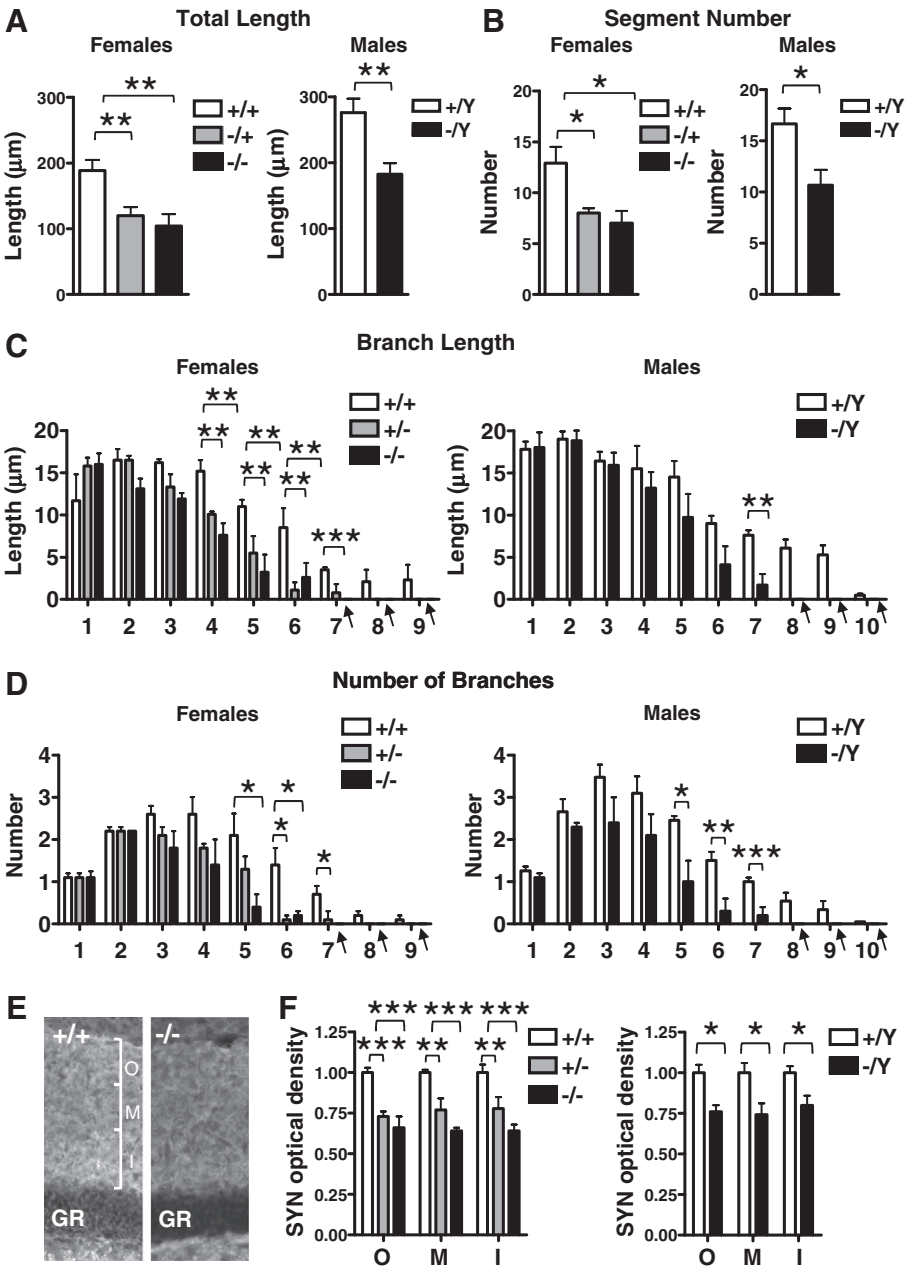

Fig. 6. Dendritic architecture of newborn granule cells of Cdkl5 KO mice. A–B: Mean total dendritic length (A) and mean number of dendritic segments (B) in homozygous (−/−; n = 5), heterozygous (+/−; n = 4) and wild type (+/+; n = 4) Cdkl5 KO female mice (panels on the left) and hemizygous (−/Y; n = 4) and wild type (+/Y; n = 4) Cdkl5 KO male mice (panels on the right). C–D: Quantification of the mean length (C) and mean number (D) of branches of the different orders in the same animals as in A. The arrows indicate the absence of branches in Cdkl5 KO mice. E: Images of sections processed for synaptophysin (SYN) immunofluorescence from the dentate gyrus of homozygous (−/−) and wild type (+/+) Cdkl5 KO female mice. Scale bar = 50 µm. G: Optical density of SYN immunoreactivity in the outer (O), middle (M) and inner (I) third of the molecular layer of the same animals as in A. Data are given as fold difference compared to the corresponding zone of the molecular layer of wild type mice. Values in A–D and F represent mean ± SD. *p < 0.05; **p < 0.01; ***p < 0.001 (Bonferroni's test after ANOVA).

ANOVA; Fig. 8D), while there was no difference in the number of astrocytes (Fig. 8D). A reduction in the number of new neurons was also found in Cdkl5 +/− mice (−67 ± 11.1 %; p < 0.01 Bonferroni's test after ANOVA; data not shown). This confirms that an absence of CDKL5 specifically decreases the survival of postmitotic neurons. Assessment of neurite outgrowth in β-tubulin III positive cells revealed that neurons generated from Cdkl5 −/− NPCs were less differentiated in comparison with wild type neurons (−40 ± 6.9%, p < 0.01, Bonferroni's test after ANOVA; Fig. 8D). A reduction in neurite length was also found in Cdkl5 +/− NPCs (−35 ± 8.1 %; p < 0.05 Bonferroni's test after ANOVA; data not shown). These results confirm that postmitotic NPCs from Cdkl5 KO mice have an intrinsic defect, not only in cell survival, but also in neuronal maturation. Evaluation of the AKT/GSK-3β pathway activation in cultures of Cdkl5 KO NPCs showed lower levels of phosphorylated AKT and GSK-3β (Fig. 8E).

In order to obtain evidence that the neurodevelopmental defects observed in Cdkl5 KO mice and Cdkl5 KO NPCs were due to a loss of Cdkl5, we re-expressed Cdkl5 in cultures of NPCs. We found that an adenovirus-mediated expression of Cdkl5 in NPCs from Cdkl5 KO mice (Fig. 8B) restored cell proliferation (Fig. 8B), neuronal survival and maturation (Fig. 8C, D). Importantly, we also found a parallel restoration of the phosphorylation levels of AKT and GSK-3β (Fig. 8E), confirming

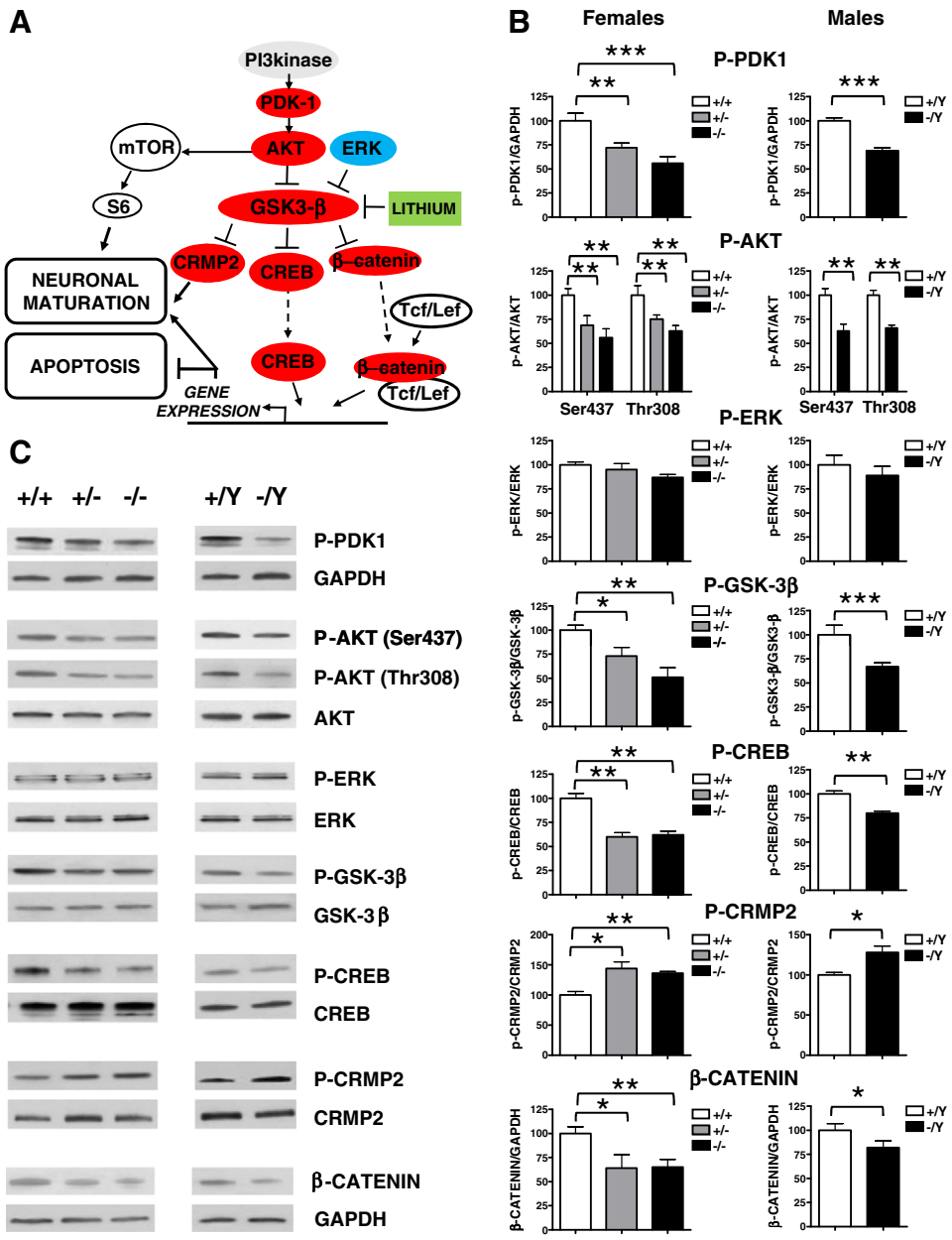

Fig. 7. AKT/GSK-3β pathway in the dentate gyrus of Cdkl5 KO mice. A: Diagram of the AKT/GSK-3β signaling cascade. The proteins indicated in red showed significantly altered phosphorylation or expression levels whereas the protein labeled in blue did not show a significant alteration in Cdkl5 KO in comparison with wild type mice. Lithium, an inhibitor of GSK-3β, is colored green. B–C: Western blot analysis of P-PDK1, P-AKT (Ser437, Thr308), P-ERK, P-GSK-3β, P-GSK-3β (Ser9), P-CREB (Ser133), P-CRMP2 (Thr514) and β-catenin levels in hippocampal homogenates of homozygous (−/−; n = 5), heterozygous (+/−; n = 5) and wild type (+/+; n = 6) Cdkl5 KO female mice and hemizygous (−/Y; n = 5) and wild type (+/Y; n = 6) Cdkl5 KO male mice. Western immunoblots in B are examples from animals of each experimental group. Histograms in C show P-AKT, P-ERK, P-GSK-3β, P-CREB and P-CRMP2 protein levels, normalized to corresponding total protein levels, and P-PDK1 and β-catenin levels, normalized to GAPDH. Data are expressed as fold difference in comparison with wild type mice. Values represent mean ± SD. *p < 0.05; **p < 0.01; ***p < 0.001 (Bonferroni's test after ANOVA).

the hypothesized link between CDKL5 and the AKT/GSK-3β pathway. Next, we treated Cdkl5 KO NPCs with an inhibitor of GSK3β activity. We used lithium, a well-known inhibitor of GSK3β activity that acts both indirectly, by increasing the inhibitory phosphorylation of GSK-3β, and directly, by antagonizing its kinase activity (Jope, 2003). We found that, in NPCs from Cdkl5 KO mice, the lithium-induced increase in the GSK-3β phosphorylation (Fig. 8E) was accompanied by a complete restoration of neuronal survival, number of new neurons and neuronal maturation (Fig. 8C, D). These data suggest that the alteration of AKT/GSK-3β signaling due to a loss of CDKL5 expression plays a role in the developmental alterations observed in Cdkl5 KO mice.

Loss of Cdkl5 impairs hippocampus-dependent behavior

In order to examine the functional correlate of the developmental abnormalities observed in the hippocampus of Cdkl5 KO mice, we evaluated spatial working memory by using the Y-maze paradigm. This test assesses the working memory, preferentially exploring the prefrontal cortex–hippocampus network (Paul et al., 2009), and is widely used to examine the impact of adult neurogenesis on hippocampus-dependent memory tasks (Hou et al., 2013). The percentage of spontaneous alternation was calculated as an index of spatial working memory. We found that while wild type mice

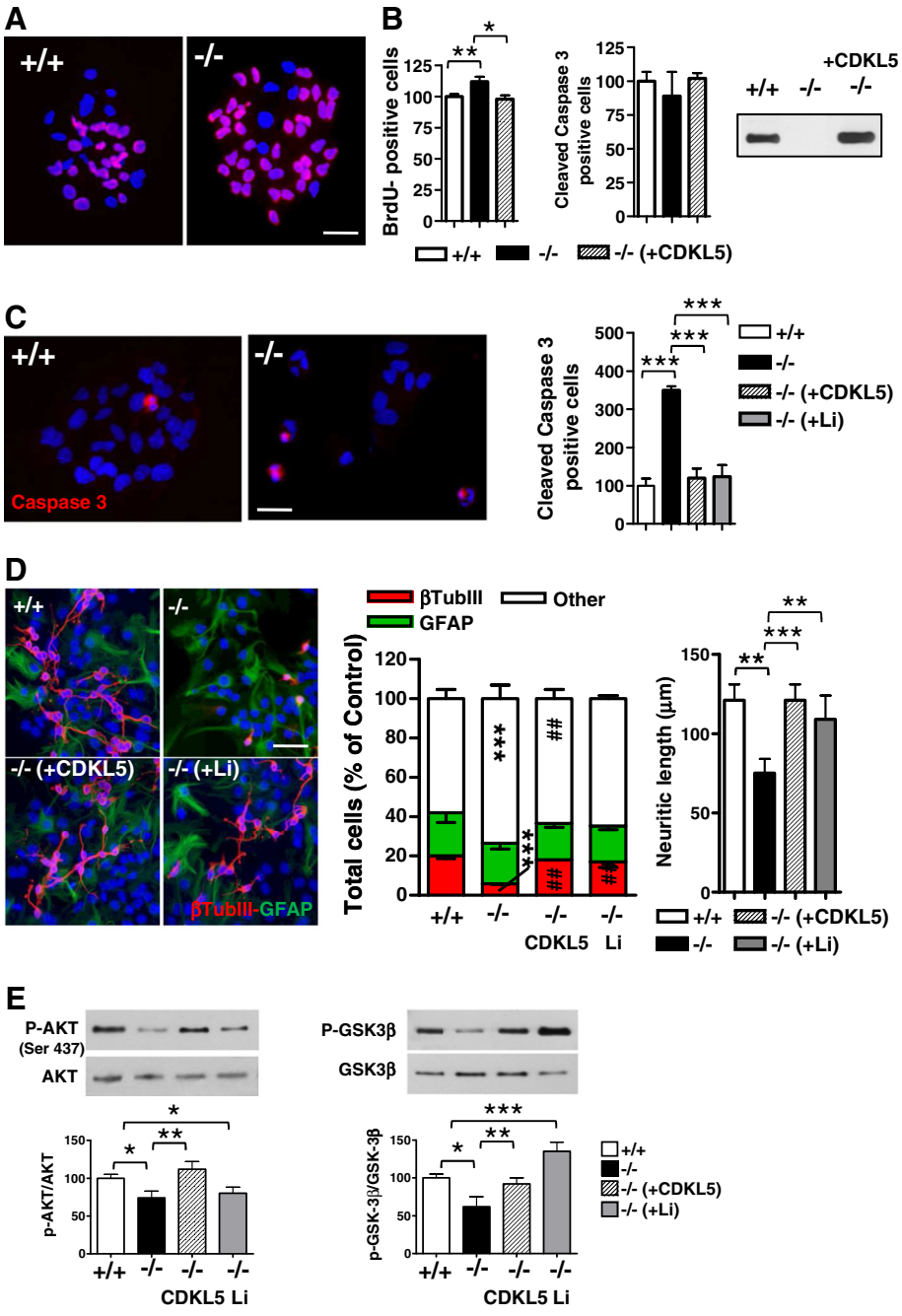

Fig. 8. Proliferation, apoptotic cell death and differentiation of cultured NPCs from the subventricular zone of Cdkl5 KO mice. A: Examples of NPCs, grown as neurospheres, from wild type (+/+) and Cdkl5 KO (−/−) mice showing BrdU-positive cells (red). Cell nuclei were stained using Hoechst dye (blue). BrdU (10 μM) was added for 16 h and thereafter cells were processed for BrdU immunohistochemistry. Scale bar = 40 μm. B: Number of BrdU-positive cells (left histogram) and cleaved caspase-3 positive cells (right histogram) over total cell number in wild type (+/+) and Cdkl5 KO (−/−) neurospheres and in Cdkl5 KO (−/−) neurospheres infected with CDKL5 adenovirus particles (MOI: 100). Example of a Western blot showing Cdkl5 expression in wild type (+/+), Cdkl5 KO (−/−) neurospheres and Cdkl5 KO (−/−) neurospheres infected with CDKL5 adenovirus particles are shown on the right. C: Images of cleaved caspase-3 positive cells in wild type (+/+) and Cdkl5 KO (−/−) NPCs after 1 day in differentiating culture conditions. Scale bar = 25 μm. Quantification of the number of cleaved caspase-3 positive cells in wild type (+/+) and Cdkl5 KO (−/−) NPCs and in Cdkl5 KO (−/−) NPCs infected with CDKL5 adenovirus particles (MOI: 100) or treated with lithium (Li; 2 mM). D: Phenotype and neuritic length of 6-days-differentiated wild type (+/+) and Cdkl5 KO (−/−) NPCs and Cdkl5 KO (−/−) NPCs infected with CDKL5 adenovirus particles (MOI: 100) or treated with lithium (2 mM). Double-fluorescence images of differentiated NPCs are reported for each experimental condition. Cells with a neuronal phenotype are immunopositive for β-tubulin III (red) and cells with an astrocytic phenotype are immunopositive for GFAP (green). Cell nuclei were stained using Hoechst dye (blue). Scale bar = 40 μm. The stacked column chart on the left represents the percentage of β-tubulin III positive cells, GFAP positive cells and cells with an undetermined phenotype (Other) over total cell number. The histogram on the right shows the quantification of neurite length. The symbol * indicates a significant difference in comparison with wild type cultures (***$p < 0.001$) and the symbol # indicates a significant difference in comparison with untreated Cdkl5 KO (#$p < 0.05$, ##$p < 0.01$); Bonferroni's test after ANOVA. E: Western blot quantification of P-AKT (Ser437) and P-GSK-3β (Ser9) levels, normalized to corresponding total protein levels, in 6 day-differentiated wild type (+/+) and Cdkl5 KO (−/−) NPCs and Cdkl5 KO (−/−) NPCs infected with CDKL5 adenovirus particles (MOI: 100) or treated with lithium (2 mM). Data in B, C and E are expressed as a percentage of wild type cultures. Values in B–E represent mean ± SE. *$p < 0.05$; **$p < 0.01$; ***$p < 0.001$ (Bonferroni's test after ANOVA).

entered more frequently into the novel, previously unvisited arm of the maze (Fig. 9A), Cdkl5 KO mice showed no preference toward the novel arm and entered randomly into the different arms approximately with the same frequency (Fig. 9A). It is to be noted that this difference was not due to a reduced motility, because Cdkl5 KO mice traveled the same distance as wild type mice (Fig. 9B). These results suggest that mice lacking Cdkl5 have deficits in spatial working memory.

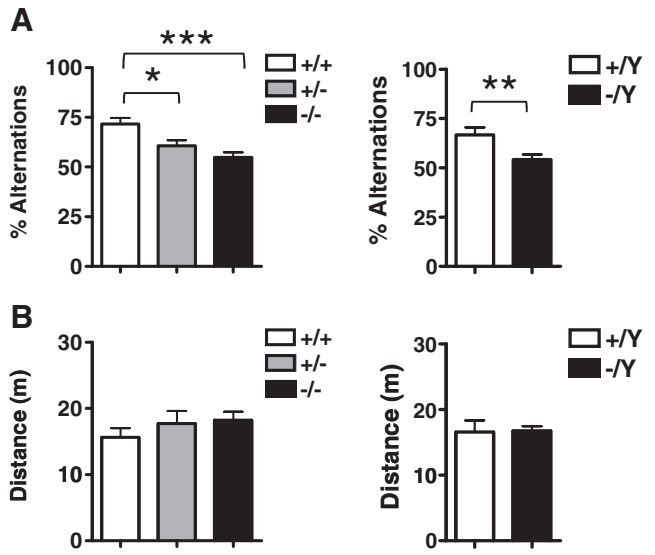

Fig. 9. Working memory test in Cdkl5 KO mice. A: Homozygous (−/−; n = 17), heterozygous (+/−; n = 11) and wild type (+/+; n = 5) Cdkl5 KO female mice and hemizygous (−/Y; n = 28) and wild type (+/Y; n = 6) Cdkl5 KO male mice were tested in a single trial Y maze task, to measure arm alternation. The percentage of spontaneous alternations is defined as (total alternations/total arm entries − 2) × 100. B: Motor activity during testing is shown as the distance traveled during the task. All data are presented as mean ± SEM. *p < 0.05; **p < 0.01; ***p < 0.001 (Dunnett's test after ANOVA).

Table 1
Summary of the effects of Cdkl5 loss on Cdkl5 KO mice.

P45 mice						
Genotype		+/+	+/−		+/Y	−/Y
Measure	Region			>	=	
Proliferation	DG	=	≥	>	=	>
	SVZ	=	>	>	=	>
Cell death	DG	=	>	>	=	>
	SVZ	=	>	=	=	>
Cell death (type 1/2a cells)	DG	=	=	=	=	=
Cell death (type 2b/3 cells)	DG	=	=	>	=	=
Cell death (immature neurons)	DG	=	>	=	=	>
Volume	DG	=	=	<	=	=
Cellularity	DG	=	<	<	=	<
Dendrites (length and number)	DG	=	<	<	=	<
SYN levels	Mol	=	<	<	=	<
pPDK1 levels	HF	=	<	<	=	<
pAKT levels	HF	=	<	<	=	<
pGSK3-β levels	HF	=	<	=	=	<
pERK levels	HF	=	=	<	=	=
pCREB levels	HF	=	<	>	=	<
pCRMP2 levels	HF	=	>	<	=	>
β -catenin levels	HF	=	<			<

P75 mice						
Genotype		+/+	+/−	−/−	+/Y	−/Y
Measure	Region					
No. of surviving cells	DG	=	<	<	=	<
No. of new neurons	DG	=	<	<	=	<
No. of new astrocytes	DG	=	=	=	=	=
Volume	DG	=	=	=	=	=
Cellularity	DG	=	<	<	=	<
Dendrites (length and number)	DG	=	<	<	=	<

Effect of genotype on different aspects of brain development (Measure column) in mice aged 45 days (P45) and 75 days (P75). These mice were the progeny of Cdkl5 KO +/− females crossed with Cdkl5 KO Y/− males or Cdkl5 KO +/− females with Y/+ males. The regions where the different measurements were carried out are indicated (Region column). The effect of genotype refers to the corresponding gender wild type Cdkl5 KO mice (+/+; +/Y). The symbols < and > indicate a lower and higher value, respectively, in comparison with wild type Cdkl5 KO mice. The symbol ≥ indicates a higher but not significant value while the symbol = indicates a value similar to that of wild type Cdkl5 KO mice. Abbreviations: DG, dentate gyrus; HF, hippocampal formation; Mol, molecular layer of the DG; SVZ, subventricular zone.

Discussion

The role of CDKL5 regarding brain development is still largely unknown. In this study, we provide novel evidence that CDKL5 plays a fundamental role in postnatal neurogenesis, by affecting neural precursor proliferation as well as the survival and maturation of newborn neurons (Table 1).

CDKL5 promotes the survival and maturation of postmitotic neurons

In the hippocampal SGZ, primary progenitor cells (type-1) produce intermediate progenitor cells (IPCs), which are a type of transit amplifying cell. Undifferentiated IPCs (type-2a and type-2b) divide rapidly to produce neuronal committed IPCs (type-3). Type-3 IPCs generate immature neurons that integrate into the hippocampal circuits as mature granule cells within 1 month (Fig. 10). The majority of these immature neurons are subjected to a selection process, during which they are either recruited into function or eliminated (Biebl et al., 2000). We found here that Cdkl5 loss caused an increase in apoptotic cell death of immature neurons with no effect on IPCs (see Fig. 4B), suggesting that CDKL5 plays a pro-survival role toward postmitotic granule neurons. We additionally found that differentiating (postmitotic) NPCs from the SVZ of Cdkl5 KO mice underwent an increase in cell death, suggesting a generalized role of CDKL5 in the survival of immature neurons in different brain regions. Previous observations showed that CDKL5 undergoes an expression increase in differentiating neurons (Valli et al., 2012), consistently with its pro-survival role in postmitotic neurons suggested by the current study. We found that while the loss of CDKL5 specifically causes the death of immature neurons, it increases proliferation rate of IPCs (see Figs. 1 and 4). The latter finding is in agreement with previous evidence showing an anti-proliferative role of this gene in neural precursor cells (Valli et al., 2012). Evaluation of the total number of granule cells in the DG showed that Cdkl5 KO mice were characterized by hypocellularity, indicating that the process of apoptotic cell death of immature granule neurons overrides the proliferation increase of their progenitors. Regarding the process of astrogliogenesis we found that a loss of Cdkl5 did not change the number of cells that acquired an astrocytic phenotype. This is in agreement with the low expression of CDKL5 in astrocytes in comparison with neurons (Rusconi et al., 2008). Taken together, these data suggest that CDKL5 plays an important role in the process of neurogenesis, but not in astrogliogenesis.

Dendritic arborization is significantly reduced in cortical pyramidal neurons from both RTT subjects (Armstrong et al., 1999; Belichenko et al., 2008, 2009) and Mecp2 knockout mice (Kishi and Macklis, 2005; Stuss et al., 2012). It is not known whether similar deficits exist in the brains of subjects carrying CDKL5 mutations. We previously showed that dendritic arborization is significantly reduced in cortical pyramidal neurons and hippocampal neurons in the Cdkl5 KO mouse model (Amendola et al., 2014), suggesting that this gene has a role in dendritic development and/or stabilization. Taking advantage of the mainly postnatal generation of hippocampal granule cells, we examined here the dendritic pattern of newly-generated granule neurons (see Fig. 6). We found that a loss of Cdkl5 causes dendritic hypotrophy, mainly due to a lack of dendritic branches of higher order. This suggests that CDKL5 plays an important role in the regulation of dendritic development. The finding that Cdkl5 KO mice had reduced SYN levels in the molecular layer of the DG suggests a reduction in the number of synaptic terminals, which is consistent with the reduced dendritic surface of granule cells.

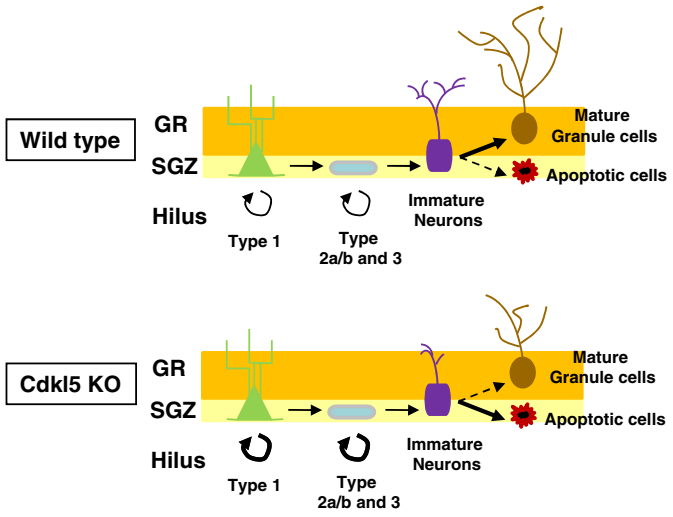

Fig. 10. Hypothetical model of CDKL5 function in postnatal hippocampus development. Top: In the normal dentate gyrus, primary progenitor cells (type 1) and intermediate progenitor cells (type 2a/b and type 3 cells) continue to proliferate, maintaining the normal progenitor pool. Postmitotic immature neurons differentiate into mature granule cells. Some of the immature neurons are committed to die. Bottom: A loss of Cdkl5 increases the proliferation rate of type 1, type 2a/b and type 3 cells but causes an increase in cell death of immature neurons, with a reduction in the final number of mature granule cells. Moreover immature neurons exhibit a hypotrophic dendritic tree.

Loss of CDKL5 impairs hippocampus-dependent memory

Results from several laboratories suggest that adult hippocampal neurogenesis is functional and is involved in learning and memory performance (Castilla-Ortega et al., 2011; Vadodaria and Jessberger, 2014). It is well established that inhibition of hippocampal neurogenesis impairs learning and memory (Pan et al., 2012; Shors et al., 2001), while stimulation of neurogenesis enhances cognitive performance, and increased neurogenesis improves the LTP of synaptic transmission (Jun et al., 2012; van Praag et al., 1999). Dendritic pathology is a possible substrate for mental retardation in different conditions. In RTT, the pathogenesis of dendritic abnormalities is distinctive and appears to correlate with the cognitive profile. We have shown that Cdkl5 KO mice not only exhibit an impaired neurogenic capacity but also a severe dendritic hypotrophy. Consistently with these neuroanatomical defects, Cdkl5 KO mice exhibited impairment in hippocampus-dependent memory. Given that cortical areas share the same defects observed here in the hippocampus of Cdkl5 KO mice, this may explain the severe cognitive impairment of individuals with CDKL5 mutations.

AKT/GSK-3β signaling plays a central role in the CDKL5-dependent regulation of neurogenesis and dendritic development

AKT/GSK-3β signaling regulates diverse developmental events in the brain, including neurogenesis, neuron survival and differentiation (Luo, 2012). For example, activation of GSK-3β promotes apoptotic signaling in cultured neural precursor cells (Eom et al., 2007), and neuronal overexpression of GSK-3β causes delayed postnatal maturation and differentiation of neurons in the mouse brain (Spittaels et al., 2000, 2002). We found that the neurogenesis and neuron maturation defects due to Cdkl5 loss were associated with impairment of the AKT/GSK-3β signaling pathway. Re-expression of CDKL5 restored NPC proliferation, survival and differentiation with a parallel restoration of the AKT/GSK-3β signaling. These results strongly suggest that a loss of Cdkl5 impairs neuron survival and maturation by disrupting the AKT/GSK-3β signaling pathway. This conclusion is strengthened by the observation that reinstatement of GSK-3β phosphorylation (inactivation) in Cdkl5 KO NPCs through the administration of lithium results in the full recovery of neuronal precursor survival and maturation. In view of the indirect action of lithium on other cellular signaling pathways (Kang et al., 2003; Pardo et al., 2003; Sasaki et al., 2006), a contribution of additional pathways cannot be ruled out. Signaling alterations of AKT/mTOR/rpS6 have recently been identified in Cdkl5 KO mouse models (Amendola et al., 2014; Wang et al., 2012), suggesting that CDKL5 may coordinate multiple signaling cascades downstream to AKT. It remains to be established whether these signaling cascades are directly or indirectly engaged by CDKL5. Together, these data suggest a central role of the AKT/GSK-3β signaling pathway in the CDKL5-dependent regulation of neurogenesis and neuron maturation and point toward the AKT/GSK-3β pathways as a potential therapeutic target for the treatment of CDKL5-related disorders.

Mosaic loss of Cdkl5 is sufficient to impair brain phenotype

Mammalian female cells randomly inactivate one of the two X chromosomes in somatic cells, and the genes on the inactive X chromosome (with a few exceptions) are not expressed. X-chromosome inactivation (XCI) occurs before the completion of gastrulation during early embryonic development and is believed to be irreversible (Plath et al., 2002). Most CDKL5 patients are females who are heterozygous for CDKL5 deficiency due to random XCI. In the current study we examined not only the phenotype of heterozygous Cdkl5 KO female mice, that mimics that of CDKL5 female patients, but also the phenotype of homozygous female and hemizygous male Cdkl5 KO mice. We found that a loss of Cdkl5 in heterozygous female mice caused decreased survival and aberrant dendritic development of newly generated granule cells and behavioral impairment. This indicates that a mosaic loss of CDKL5 in 50% of cells in the brain alters neuronal survival/differentiation in a manner that is sufficient to impair cognitive performance. As expected, homozygous female and hemizygous male mice had a more severe brain phenotype due to Cdkl5 loss in 100% of cells.

Conclusion

Taken together, our data suggest that CDKL5 modulates the intricate balance between precursor proliferation/survival and differentiation during the process of postnatal neurogenesis (Fig. 10). It is worth noting that the phenotype of Cdkl5 knockout mice only partially overlaps with that of Mecp2 knockouts. While both mutants show severe dendritic hypotrophy (Amendola et al., 2014; Smrt et al., 2007), there is no evidence for altered neural precursor proliferation and survival in Mecp2 KO mice. Translation of this evidence to the human condition suggests that dendritic hypotrophy may explain common phenotypic features in individuals with CDKL5 disorder and RTT. On the other hand, reduction in neuron survival appears to be a typical feature of CDKL5 disorder that may explain phenotypes that are not shared with RTT.

We suggest that a loss of Cdkl5 impairs neurogenesis and dendritic development by disrupting the AKT/GSK-3β signaling pathway. Disruption of neurogenesis and dendritic development in the hippocampus leads to alterations in cognitive performance. The transfer of these data to the human pathology suggests that a generalized impairment of key processes of brain development may underlie the generalized and severe cognitive impairment in individuals with CDKL5 disorder.

Supplementary data to this article can be found online at http://dx.doi.org/10.1016/j.nbd.2014.06.006.

Acknowledgments

This work was supported by the Telethon grant (GGP11147) to EC and LC, by the "CDKL5 associazione di volontariato" to EC, by the International Foundation for CDKL5 Research (IFCR) in collaboration with ISRF to EA and by EMBL to CG.

References

Aimone, J.B., Deng, W., Gage, F.H., 2010. Adult neurogenesis: integrating theories and separating functions. Trends Cogn. Sci. 14, 325–337.

Amendola, E., Zhan, Y., Mattucci, C., Castroflorio, E., Calcagno, E., Fuchs, C., Lonetti, G., Silingardi, D., Farley, D., Ciani, E., Pizzorusso, T., Giustetto, M., Gross, C.T., 2014. Mapping pathological phenotypes in a mouse model of CDKL5 disorder. PLoS One 16 (9(5)), e91613.

Armstrong, D.D., Dunn, J.K., Schultz, R.J., Herbert, D.A., Glaze, D.G., Motil, K.J., 1999. Organ growth in Rett syndrome: a postmortem examination analysis. Pediatr. Neurol. 20, 125–129.

Bahi-Buisson, N., Kaminska, A., Boddaert, N., Rio, M., Afenjar, A., Gerard, M., Giuliano, F., Motte, J., Heron, D., Morel, M.A., Plouin, P., Richelme, C., des Portes, V., Dulac, O., Philippe, C., Chiron, C., Nabbout, R., Bienvenu, T., 2008a. The three stages of epilepsy in patients with CDKL5 mutations. Epilepsia 49, 1027–1037.

Bahi-Buisson, N., Nectoux, J., Rosas-Vargas, H., Milh, M., Boddaert, N., Girard, B., Cances, C., Ville, D., Afenjar, A., Rio, M., Heron, D., N'Guyen Morel, M.A., Arzimanoglou, A., Philippe, C., Jonveaux, P., Chelly, J., Bienvenu, T., 2008b. Key clinical features to identify girls with CDKL5 mutations. Brain 131, 2647–2661.

Bahi-Buisson, N., Villeneuve, N., Caietta, E., Jacquette, A., Maurey, H., Matthijs, G., Van Esch, H., Delahaye, A., Moncla, A., Milh, M., Zufferey, F., Diebold, B., Bienvenu, T., 2012. Recurrent mutations in the CDKL5 gene: genotype-phenotype relationships. Am. J. Med. Genet. A 158A, 1612–1619.

Belichenko, N.P., Belichenko, P.V., Li, H.H., Mobley, W.C., Francke, U., 2008. Comparative study of brain morphology in Mecp2 mutant mouse models of Rett syndrome. J. Comp. Neurol. 508, 184–195.

Belichenko, N.P., Belichenko, P.V., Mobley, W.C., 2009. Evidence for both neuronal cell autonomous and nonautonomous effects of methyl-CpG-binding protein 2 in the cerebral cortex of female mice with Mecp2 mutation. Neurobiol. Dis. 34, 71–77.

Bertani, I., Rusconi, L., Bolognese, F., Forlani, G., Conca, B., De Monte, L., Badaracco, G., Landsberger, N., Kilstrup-Nielsen, C., 2006. Functional consequences of mutations in CDKL5, an X-linked gene involved in infantile spasms and mental retardation. J. Biol. Chem. 281, 32048–32056.

Bianchi, P., Ciani, E., Guidi, S., Trazzi, S., Felice, D., Grossi, G., Fernandez, M., Giuliani, A., Calza, L., Bartesaghi, R., 2010. Early pharmacotherapy restores neurogenesis and cognitive performance in the Ts65Dn mouse model for Down syndrome. J. Neurosci. 30, 8769–8779.

Biebl, M., Cooper, C.M., Winkler, J., Kuhn, H.G., 2000. Analysis of neurogenesis and programmed cell death reveals a self-renewing capacity in the adult rat brain. Neurosci. Lett. 291, 17–20.

Castilla-Ortega, E., Pedraza, C., Estivill-Torrus, G., Santin, L.J., 2011. When is adult hippocampal neurogenesis necessary for learning? evidence from animal research. Rev. Neurosci. 22, 267–283.

Cheadle, J.P., Gill, H., Fleming, N., Maynard, J., Kerr, A., Leonard, H., Krawczak, M., Cooper, D.N., Lynch, S., Thomas, N., Hughes, H., Hulten, M., Ravine, D., Sampson, J.R., Clarke, A., 2000. Long-read sequence analysis of the MECP2 gene in Rett syndrome patients: correlation of disease severity with mutation type and location. Hum. Mol. Genet. 9, 1119–1129.

Chen, Q., Zhu, Y.C., Yu, J., Miao, S., Zheng, J., Xu, L., Zhou, Y., Li, D., Zhang, C., Tao, J., Xiong, Z. Q., 2010. CDKL5, a protein associated with rett syndrome, regulates neuronal morphogenesis via Rac1 signaling. J. Neurosci. 30, 12777–12786.

Cole, A.R., 2012. GSK3 as a sensor determining cell fate in the brain. Front. Mol. Neurosci. http://dx.doi.org/10.3389/fnmol.2012.00004.

Contestabile, A., Fila, T., Ceccarelli, C., Bonasoni, P., Bonapace, L., Santini, D., Bartesaghi, R., Ciani, E., 2007. Cell cycle alteration and decreased cell proliferation in the hippocampal dentate gyrus and in the neocortical germinal matrix of fetuses with Down syndrome and in Ts65Dn mice. Hippocampus 17, 665–678.

Contestabile, A., Fila, T., Bartesaghi, R., Ciani, E., 2009. Cell cycle elongation impairs proliferation of cerebellar granule cell precursors in the Ts65Dn mouse, an animal model for Down syndrome. Brain Pathol. 19, 224–237.

Eom, T.Y., Roth, K.A., Jope, R.S., 2007. Neural precursor cells are protected from apoptosis induced by trophic factor withdrawal or genotoxic stress by inhibitors of glycogen synthase kinase 3. J. Biol. Chem. 282, 22856–22864.

Evans, J.C., Archer, H.L., Colley, J.P., Ravn, K., Nielsen, J.B., Kerr, A., Williams, E., Christodoulou, J., Gecz, J., Jardine, P.E., Wright, M.J., Pilz, D.T., Lazarou, L., Cooper, D.N., Sampson, J.R., Butler, R., Whatley, S.D., Clarke, A.J., 2005. Early onset seizures and Rett-like features associated with mutations in CDKL5. Eur. J. Hum. Genet. 13, 1113–1120.

Goto, T., Monk, M., 1998. Regulation of X-chromosome inactivation in development in mice and humans. Microbiol. Mol. Biol. Rev. 62, 362–378.

Grimes, C.A., Jope, R.S., 2001. CREB DNA binding activity is inhibited by glycogen synthase kinase-3 beta and facilitated by lithium. J. Neurochem. 78, 1219–1232.

Guerrini, R., Parrini, E., 2012. Epilepsy in Rett syndrome, and CDKL5- and FOXG1-gene-related encephalopathies. Epilepsia 53, 2067–2078.

Hou, J.G., Xue, J.J., Lee, M.R., Sun, M.Q., Zhao, X.H., Zheng, Y.N., Sung, C.K., 2013. Compound K is able to ameliorate the impaired cognitive function and hippocampal neurogenesis following chemotherapy treatment. Biochem. Biophys. Res. Commun. 436, 104–109.

Jope, R.S., 2003. Lithium and GSK-3: one inhibitor, two inhibitory actions, multiple outcomes. Trends Pharmacol. Sci. 24, 441–443.

Jun, H., Mohammed Qasim Hussaini, S., Rigby, M.J., Jang, M.H., 2012. Functional role of adult hippocampal neurogenesis as a therapeutic strategy for mental disorders. Neural Plast. 854285.

Kameshita, I., Sekiguchi, M., Hamasaki, D., Sugiyama, Y., Hatano, N., Suetake, I., Tajima, S., Sueyoshi, N., 2008. Cyclin-dependent kinase-like 5 binds and phosphorylates DNA methyltransferase 1. Biochem. Biophys. Res. Commun. 377, 1162–1167.

Kang, H.J., Noh, J.S., Bae, Y.S., Gwag, B.J., 2003. Calcium-dependent prevention of neuronal apoptosis by lithium ion: essential role of phosphoinositide 3-kinase and phospholipase Cgamma. Mol. Pharmacol. 64, 228–234.

Kempermann, G., Jessberger, S., Steiner, B., Kronenberg, G., 2004. Milestones of neuronal development in the adult hippocampus. Trends Neurosci. 27, 447–452.

Kishi, N., Macklis, J.D., 2005. Dissecting MECP2 function in the central nervous system. J. Child Neurol. 20, 753–759.

Lowry, O.H., Rosebrough, N.J., Farr, A.L., Randall, R.J., 1951. Protein measurement with the Folin phenol reagent. J. Biol. Chem. 193, 265–275.

Luo, J., 2012. The role of GSK3beta in the development of the central nervous system. Front. Biol. 7, 212–220.

Mari, F., Azimonti, S., Bertani, I., Bolognese, F., Colombo, E., Caselli, R., Scala, E., Longo, I., Grosso, S., Pescucci, C., Ariani, F., Hayek, G., Balestri, P., Bergo, A., Badaracco, G., Zappella, M., Broccoli, V., Renieri, A., Kilstrup-Nielsen, C., Landsberger, N., 2005. CDKL5 belongs to the same molecular pathway of MeCP2 and it is responsible for the early-onset seizure variant of Rett syndrome. Hum. Mol. Genet. 14, 1935–1946.

O'Kusky, J.R., Ye, P., D'Ercole, A.J., 2000. Insulin-like growth factor-I promotes neurogenesis and synaptogenesis in the hippocampal dentate gyrus during postnatal development. J. Neurosci. 20, 8435–8442.

Pan, Y.W., Chan, G.C., Kuo, C.T., Storm, D.R., Xia, Z., 2012. Inhibition of adult neurogenesis by inducible and targeted deletion of ERK5 mitogen-activated protein kinase specifically in adult neurogenic regions impairs contextual fear extinction and remote fear memory. J. Neurosci. 32, 6444–6455.

Pardo, R., Andreolotti, A.G., Ramos, B., Picatoste, F., Claro, E., 2003. Opposed effects of lithium on the MEK-ERK pathway in neural cells: inhibition in astrocytes and stimulation in neurons by GSK3 independent mechanisms. J. Neurochem. 87, 417–426.

Paul, C.M., Magda, G., Abel, S., 2009. Spatial memory: theoretical basis and comparative review on experimental methods in rodents. Behav. Brain Res. 203, 151–164.

Plath, K., Mlynarczyk-Evans, S., Nusinow, D.A., Panning, B., 2002. Xist RNA and the mechanism of X chromosome inactivation. Annu. Rev. Genet. 36, 233–278.

Ricciardi, S., Ungaro, F., Hambrock, M., Rademacher, N., Stefanelli, G., Brambilla, D., Sessa, A., Magagnotti, C., Bachi, A., Giarda, E., Verpelli, C., Kilstrup-Nielsen, C., Sala, C., Kalscheuer, V.M., Broccoli, V., 2012. CDKL5 ensures excitatory synapse stability by reinforcing NGL-1-PSD95 interaction in the postsynaptic compartment and is impaired in patient iPSC-derived neurons. Nat. Cell Biol. 14, 911–923.

Rusconi, L., Salvatoni, L., Giudici, L., Bertani, I., Kilstrup-Nielsen, C., Broccoli, V., Landsberger, N., 2008. CDKL5 expression is modulated during neuronal development and its subcellular distribution is tightly regulated by the C-terminal tail. J. Biol. Chem. 283, 30101–30111.

Sasaki, T., Han, F., Shioda, N., Moriguchi, S., Kasahara, J., Ishiguro, K., Fukunaga, K., 2006. Lithium-induced activation of Akt and CaM kinase II contributes to its neuroprotective action in a rat microsphere embolism model. Brain Res. 1108, 98–106.

Scala, E., Ariani, F., Mari, F., Caselli, R., Pescucci, C., Longo, I., Meloni, I., Giachino, D., Bruttini, M., Hayek, G., Zappella, M., Renieri, A., 2005. CDKL5/STK9 is mutated in Rett syndrome variant with infantile spasms. J. Med. Genet. 42, 103–107.

Sekiguchi, M., Katayama, S., Hatano, N., Shigeri, Y., Sueyoshi, N., Kameshita, I., 2013. Identification of amphiphysin 1 as an endogenous substrate for CDKL5, a protein kinase associated with X-linked neurodevelopmental disorder. Arch. Biochem. Biophys. 535, 257–267.

Shors, T.J., Miesegaes, G., Beylin, A., Zhao, M., Rydel, T., Gould, E., 2001. Neurogenesis in the adult is involved in the formation of trace memories. Nature 410, 372–376.

Smrt, R.D., Eaves-Egenes, J., Barkho, B.Z., Santistevan, N.J., Zhao, C., Aimone, J.B., Gage, F.H., Zhao, X., 2007. Mecp2 deficiency leads to delayed maturation and altered gene expression in hippocampal neurons. Neurobiol. Dis. 27, 77–89.

Spittaels, K., Van den Haute, C., Van Dorpe, J., Geerts, H., Mercken, M., Bruynseels, K., Lasrado, R., Vandezande, K., Laenen, I., Boon, T., Van Lint, J., Vandenheede, J., Moechars, D., Loos, R., Van Leuven, F., 2000. Glycogen synthase kinase-3beta phosphorylates protein tau and rescues the axonopathy in the central nervous system of human four-repeat tau transgenic mice. J. Biol. Chem. 275, 41340–41349.

Spittaels, K., Van den Haute, C., Van Dorpe, J., Terwel, D., Vandezande, K., Lasrado, R., Bruynseels, K., Irizarry, M., Verhoye, M., Van Lint, J., Vandenheede, J.R., Ashton, D., Mercken, M., Loos, R., Hyman, B., Van der Linden, A., Geerts, H., Van Leuven, F., 2002. Neonatal neuronal overexpression of glycogen synthase kinase-3 beta reduces brain size in transgenic mice. Neuroscience 113, 797–808.

Stuss, D.P., Boyd, J.D., Levin, D.B., Delaney, K.R., 2012. MeCP2 mutation results in compartment-specific reductions in dendritic branching and spine density in layer 5 motor cortical neurons of YFP-H mice. PLoS One 7, e31896.

Tao, J., Van Esch, H., Hagedorn-Greiwe, M., Hoffmann, K., Moser, B., Raynaud, M., Sperner, J., Fryns, J.P., Schwinger, E., Gecz, J., Ropers, H.H., Kalscheuer, V.M., 2004. Mutations in the X-linked cyclin-dependent kinase-like 5 (CDKL5/STK9) gene are associated with severe neurodevelopmental retardation. Am. J. Hum. Genet. 75, 1149–1154.

Trazzi, S., Mitrugno, V.M., Valli, E., Fuchs, C., Rizzi, S., Guidi, S., Perini, G., Bartesaghi, R., Ciani, E., 2011. APP-dependent up-regulation of Ptch1 underlies proliferation impairment of neural precursors in Down syndrome. Hum. Mol. Genet. 20, 1560–1573.

Vadodaria, K.C., Jessberger, S., 2014. Functional neurogenesis in the adult hippocampus: then and now. Front. Neurosci. http://dx.doi.org/10.3389/fnins.2014.00055.

Valli, E., Trazzi, S., Fuchs, C., Erriquez, D., Bartesaghi, R., Perini, G., Ciani, E., 2012. CDKL5, a novel MYCN-repressed gene, blocks cell cycle and promotes differentiation of neuronal cells. Biochim. Biophys. Acta 1819, 1173–1185.

van Praag, H., Christie, B.R., Sejnowski, T.J., Gage, F.H., 1999. Running enhances neurogenesis, learning, and long-term potentiation in mice. Proc. Natl. Acad. Sci. U. S. A. 96, 13427–13431.

Wada, A., 2009. Lithium and neuropsychiatric therapeutics: neuroplasticity via glycogen synthase kinase-3beta, beta-catenin, and neurotrophin cascades. J. Pharmacol. Sci. 110, 14–28.

Wang, I.T., Allen, M., Goffin, D., Zhu, X., Fairless, A.H., Brodkin, E.S., Siegel, S.J., Marsh, E.D., Blendy, J.A., Zhou, Z., 2012. Loss of CDKL5 disrupts kinome profile and event-related potentials leading to autistic-like phenotypes in mice. Proc. Natl. Acad. Sci. U. S. A. 109, 21516–21521.

Weaving, L.S., Christodoulou, J., Williamson, S.L., Friend, K.L., McKenzie, O.L., Archer, H., Evans, J., Clarke, A., Pelka, G.J., Tam, P.P., Watson, C., Lahooti, H., Ellaway, C.J., Bennetts, B., Leonard, H., Gecz, J., 2004. Mutations of CDKL5 cause a severe neurodevelopmental disorder with infantile spasms and mental retardation. Am. J. Hum. Genet. 75, 1079–1093.

Yoshimura, T., Kawano, Y., Arimura, N., Kawabata, S., Kikuchi, A., Kaibuchi, K., 2005. GSK-3beta regulates phosphorylation of CRMP-2 and neuronal polarity. Cell 120, 137–149.

Zhu, Y.C., Li, D., Wang, L., Lu, B., Zheng, J., Zhao, S.L., Zeng, R., Xiong, Z.Q., 2013. Palmitoylation-dependent CDKL5-PSD-95 interaction regulates synaptic targeting of CDKL5 and dendritic spine development. Proc. Natl. Acad. Sci. U. S. A. 110, 9118–9123.